PERMISSIONS

"I give permission for public access to my thesis and for any copying to be done at the discretion of the archives librarian and/or the College librarian."

Signature: **Jessica C. McHale**

Date: **May 14, 2014**

ABTRACT

Fluvial and volcanic features on Mars are often difficult to distinguish just based on morphological observations. A better understanding of the possible processes that form features such as cracks that are associated with undifferentiated flows on Mars, might be helpful in determining the geological processes involved. The study of Earth analogs is one approach to better understand these features. The 3900 year old McCartys basalt pahoehoe flow is the youngest flow in the late Cenozoic Zuni-Bandera volcanic field in New Mexico (Dunbar and Phillips, 2004). The southern part of the flow includes numerous extensive plateaus that are surrounded by escarpments, mounds and dotted by pits. Cracks are widely distributed, but are particularly prevalent where slope changes occur. Previous workers have attributed many of these features to the process of inflation, or the rising of an already solidified basaltic crust due to further magma injection from below (Mabery, 1999). The goal of this study is to quantify these features within the context of the inflation model through detailed field observations, GIS mapping, and physical modeling. We distinguished three types of inflation crack patterns based on shape, crack density and crack size, which are consistent over all of the McCartys' escarpments. This study enhances our understanding of crack formation due to lava inflation and may aid in the identification of lava flow features on Mars.

BASALT INFLATION PLATEAU ESCARPMENT CRACK PATTERNS-FIELD, GIS & IMPLICATIONS FOR MARS

By Jessica Claire McHale

A thesis presented to the Faculty of Mount Holyoke College in partial fulfillment of the requirements for the Degree of Bachelor of Arts with Honors

Department of Geology and Geography
Mount Holyoke College
South Hadley, Massachusetts

May, 2014

Advisor: Michelle Markley
Committee Members: Michelle Markley, Alan Werner, and Joshua Roth
Department Chair: Michelle Markley

ACKNOWLEDGEMENTS

I would like to thank the Keck Geology Consortium for funding my field work in the Summer of 2013, as well as my Keck advisor, Andrew deWet, for his guidance in the field and technical support; my Mount Holyoke thesis advisor, Michelle Markley, for her humor, patience and editing skills; Jacob Bleacher, Brent Garry and Christopher Hamilton for their guidance in the field; my fellow Keck students, Charles Wise, Megan Switzer, Susan Konkol, Hester von Meerscheidt, and Ryan Samuels; and finally, the student, faculty, and administrators of the Mount Holyoke College Departments of Geology and Geography for their laughter, support and understanding.

TABLE OF CONTENTS

INTRODUCTION

Study Overview and Purpose

Inflation plateaus are uplifted pahoehoe sheet flows with monoclinal escarpments (Hon et al., 1994). The McCartys flow in El Malpaís National Monument, New Mexico, is an inflation plateau. During summer 2013 field work on the McCartys flow, we identified three types of escarpments. My study aims to define the three types of escarpments clearly and to explore the possibility of identifying these escarpment types on inflation plateaus on Mars. I also present my interpretations of the local histories that caused each type of escarpment to form.

Escarpment Types

Each of the three escarpment types has a different slope, trace and crack morphology. The first escarpment type, Type A, has a linear slope, linear trace and one wide crack at the top of the escarpment. The second escarpment type, Type B, has a slope that is convex in some places and concave in others, a concave trace and many narrow, subparallel cracks. The third escarpment type, Type C, has a convex slope, a convex trace, and polygonally intersecting cracks.

Mars

The surface of Mars shows extensive evidence for volcanism. Mars lavas have basaltic to ultramafic compositions, although some shield volcanoes appear to have more evolved compositions (Wilson and Head, 1994).

Mars Compared to Earth

Conductive heat transfer processes in the interiors of both Mars and Earth occur at a similar rate (Wilson and Head, 1994). Fluid convection and crystal settling processes driven by buoyancy are slower on Mars due to lower gravity; this causes slower rates of diapirism on Mars, which in turn allows larger diapirs to ascend to a shallower level in Mars than in Earth (Wilson and Head, 1994). Volcanism is common on Earth and Mars, but effusion rates are five times higher on Mars than on Earth (due to the differences in gravity), and lava flows move almost twice as fast on Mars. All of the above factors combine to create volcanic features on Mars that are many times larger than their Earth counterparts. Despite the presence of volcanism, plate tectonics has not been observed on Mars (Werner, 2009).

Mars Volcanic Features

Three types of lava flows have been observed on Mars: short and narrow, long and sheet-like, and long and tube-fed (Wilson and Head, 1994; Figure 1). Tube-fed flows are typically the longest because the insulation of liquid lava within the tubes allows for lava to be kept at high temperatures over longer distances. Lava floods are flows over large areas that have lobate boundaries and

can be up to 10m thick (Wilson and Head, 1994). Small shield volcanoes, with diameters up to 150km, are often related to dikes and fissures. Large shield volcanoes, such as Tharsis Montes and Olympus Mons, are 500-700km in diameter, and flows originating from these volcanoes can be hundreds of kilometers long and up to 25km tall, much taller than Earth counterparts. This height difference is attributed to the variations between Mars and Earth conditions that allow Martian lava flows to have lengths up to 6 times greater than analogous terrestrial flows (Wilson and Head, 1994).

Tharsis

Tharsis is one of two volcanic provinces on Mars that has morphologies similar to basaltic landforms on Earth (Werner, 2009). It is near the equator and contains large volcanoes similar to Hawaiian basaltic shield volcanoes: Olympus Mons, Ascraeus Mons, Pavonis Mons, and Arsia Mons. Mars volcanism localized to Tharsis 1.6Ga and was active as recently as 200-100Ma (Werner, 2009).

Elysium

Elysium is the second-largest volcanic province and is made up of Elysium Mons, Hecate Tholus and Albor Tholus (Werner, 2009). Some of the youngest volcanic activity, around and stemming from Elysium Mons, is 3.48Ga (Werner, 2009).

Inflation Plateaus in Elysium

There are several inflation plateaus in Elysium. One type are amoeboid raised plateaus with circular pits whose bases are the topographic surface pre-flow (Keszthelyi et al., 2008; Figure 2). Some have an extensive fairly flat surface and slanted escarpments (Figure 2). The inflation plateau has several indentations, which Keszthelyi et al. (2008) interprets as inflation pits. Hamilton (2013) took inflation plateau identification a step further by pairing images of a Martian plateau with an image of an escarpment on a terrestrial inflation plateau (Figure 3). The close-up Martian and terrestrial images focus on the typical slanted escarpments and the distinct cracks that cover the escarpments. Hauber (2009) looks at the same Martian inflation plateau as Keszthelyi et al., but he also shows a Martian tumulus (Figure 4b). Tumuli are positive, volcanic topographic features that form mounds or whaleback ridges, 1-10m high with deeply gashed systems of axial to more or less radial gaping clefts (Walker, 1991). The Martian tumulus is not flat on top like an inflation plateau, and is much smaller (Figure 4d). The terrestrial tumulus is smaller than the terrestrial inflation plateau, and appears to be a freestanding bulge of lava (Figure 4c).

Morphologically, Martian inflation plateaus are very similar to the terrestrial ones. They are a few hundred meters across and a few kilometers long, similar to the McCartys and other terrestrial inflation plateaus. Keszthelyi et al. (2008) proposed that inflation features and inflation pits form as lava moves over deep cracks because a deep fissure would have allowed for a drawn out cooling

period and latter draining of any liquid lava after most of the flow had solidified. The inflation plateaus Keszthelyi et al. (2008) examined are covered by a layer of unconsolidated material that the lava either intruded under or was laid down concurrently.

Inflation plateaus are most common with pahoehoe sheet flows (Self et al., 1998). As on Earth, the core of the flow makes up half the flow thickness on Mars (Keszthelyi et al., 2008). Keszthelyi et al. (2008) were able to discern this by identifying an inflated flow core, which is generally more resistant to erosion than the rest of the flow because the core has fewer vesicles. HiRISE imaging is necessary for confident identification of inflation plateaus (Keszthelyi et al., 2008).

Flood Lavas

Flood lavas are composed of numerous lava flows, up to 1000km in length, resulting from spillover from channelized flows (Keszthelyi et al., 2008). Their surfaces display a nobbly, brecciated texture. These floods generally moved as large sheets, but can form local lava tubes where topographically confined. Pressure ridges and shear zones often occur on the edges of these flood lavas (Figures 5 and 6). Some lava floods have a platy-ridged morphology.

Alternate Theory of Martian Inflation Plateau Formation

Keszthelyi et al. (2008) speculates that the uplifts may have been caused by freezing groundwater. The associated uplifts are gigantic permafrost pingos (Keszthelyi et al., 2008). They suggest the pingos may have formed when lava

melted the ground ice and caused the water to flow through the subsurface. They also claim that the topography of the Martian uplifts is similar to terrestrial hydraulic pingos, but on a much larger scale on Mars. Keszthelyi et al. (2008) concludes that the abrupt termination of uplift at the flow margins makes this theory weak. Inflation plateaus have abrupt edges due to the solid nature of lava, but pingo permafrost areas often have a more uniform ending due to the flow of ground water and ice.

Mars Overview

The escarpment types, this study describes and identifies on the McCartys flow, may be analogous to volcanic features on Mars identified as inflation plateaus. Escarpment types on volcanic feature edges provide a further identification method for inflation plateaus that can be applied using satellite images.

Inflation Plateaus on Earth

Below I review research based on field observations of active basaltic lava flows; many of these studies are conducted in Hawaii (Crown and Baloga, 1999; Self et al., 1998; Hon et al., 1994; Hoblitt et al., 2012). The purpose of this study is to set the stage for a detailed description of inflation features on the McCartys flow.

Pahoehoe

Inflation plateaus are composed of basaltic pahoehoe lava. Pahoehoe lava flows need sustained low rates of eruptions to form (Crown and Baloga, 1999). It has flexible skin that forms ropes and distinctive millimeter- to decimeter scale surface textures (Self et al., 1998). There are two distinct types of pahoehoe, silvery and blue-glassy. Silvery lobes are created by numerous stretched vesicles, and correspond to S-type (spongy) lobes (Self et al., 1998). Blue-glassy lobes have nearly no vesicles in the outer layers, but have large internal vesicles. Meter-scale pahoehoe lobes can coalesce laterally while inflating to form an inflation plateau that can be several meters thick and hundreds of meters wide, this process can last anywhere from days to years. The thickness of the vesicular upper crust can be used to determine how long the inflation process took (Self et al., 1998; Hon et al., 1994).

Pahoehoe lava emplaced over smooth topography forms sheet-like lobes; however, when it is emplaced over rough, steep surfaces it forms “hummocky” flows with discrete tumuli (Self et al., 1998). Inflated pahoehoe flows can

become very large because they are slow to cool because they develop a thick cool upper crust, which acts as an insulator. Liquid lava travels in such a system in tubes or pools; similar to blood flowing through veins under the skin.

Sheet Flow Advancement

Pahoehoe flows are usually tube-fed, either directly from the vent or from tube system breakouts (Crown and Baloga, 1999). Sheet flows form when pahoehoe is not confined to a channel and can spread in all directions. Sheet flow advancement rates are controlled by the strength of the viscoelastic skin and the rate liquid lava is supplied to the front of the flow (Hoblitt et al., 2012). A thin viscoelastic skin and a rapid rate of new liquid lava injection is associated with an increased rate of flow advancement.

Sheet flows advance when liquid lava emerges at or near the surface where the skin of the lobes is the thinnest (Hoblitt et al., 2012). Sheet flows can also advance through outbreaks along the inflated fronts of the flow lobes (Hon et al., 1994). The outbreaks occur when the tensile strength of the brittle crust is exceeded because of the continued input of lava. Tensile stresses in the brittle crust include cooling-induced shrinkage and the addition of liquid lava in the flow's core (Hoblitt et al., 2012). The fractures produced by tensile stresses can cause cracks that propagate downwards to the viscoelastic layer. If the viscoelastic layer's strength is exceeded the layer will ductilely fail and tear, which will allow liquid lava to escape from the inner core and form a break-out. As the still plastic-skinned lobes spread and inflate they can coalesce and form a

singular liquid interior between a cooled upper and lower crust (Hoblitt et al., 2012; Hon et al., 1994). There is no preserved boundary between inflated lobes in an inflated sheet flow because the lobes coalesce while their outer skin is still plastic.

Sheet flows are influenced by topography (Hon et al., 1994). Small obstacles (only a few centimeters tall) can halt a sheet flow causing it to inflate. Liquid lava can be stored in the core and continue to cause outbreaks even after the vent stops supplying lava (Hon et al., 1994).

Inside the lava flow the liquid lava circulates, and the lava nearest the crust is the coolest (Hon et al., 1994). The liquid lava in the interior of the flow is kept at a high temperature due to the insulation of the upper and lower solidified crusts. The temperature and hydrostatic pressure maintained by liquid lava is constantly being flushed through tube-like systems underneath the crust and occasionally being stored in pools.

Lobes and Toes

A flow lobe is a single unit of lava with a glassy crust that is decimeters to kilometers wide and up to 60 meters thick (Thordarson and Self, 1998). Pahoehoe toes have complex flow patterns because of the influence of topography and nearby toes (Crown and Baloga, 1999). Vesicles in the upper surfaces of toes stretch and act as flow direction indicators. The shape and size of lobes and toes are controlled by small-scale topography and roughness, partitioning of discharge from the vent through tubes and channels, and local fluctuations in supply rates to

lobes and toes. Lobes branch in different ways depending on topography. The first way is a thin, elongate lobe with little relief on the upper surface; these form on smooth, unconfined surfaces. The second type forms centrally ridged lobes, with thickening or a pile of toes in the center and thinning towards the lateral margins (Crown and Baloga, 1999). This second type has small-scale inflation along the center of the lobes. These lobes have irregular, ropey, upper surfaces due to increased fracturing of the inflated lobes. Overall ropey lobes tend to have more branched lobes and toes than smooth ones. Lobe and toe advancement at individual lobe scale appears fairly random; although, pahoehoe flow advancement is generally predictable in its tendencies to flow downhill and spread laterally (Crown and Baloga, 1999).

Inflation of Sheet flows

Inflated sheet flows are often called inflation plateaus due to their geomorphic appearance (Figure 7). "Inflated pahoehoe sheet flows have a distinctive horizontal upper surface, which can be several hundred meters across, and are bounded by steep monoclinal uplifts," (Hon et al., 1994). There are two main styles of flow uplift, one creates vertical scarps and the other creates tilted lava slab margins. An inflation plateau is a composite of many inflated lobes resulting a complex shape. These lobes inflate after breaking out from cracks in the front of other inflated lobes.

Sheet flows start as thin (centimeter scale) flow before the additional injection of liquid lava inflates the flows' thin, mm-scale, plastic skin. On gentle

slopes lava moves laterally at the same speed as it moves forward, which allows lobes to coalescence and form a liquid core beneath a single upper-crustal layer (Hon et al., 1994). The crust forms a horizontal insulation for the liquid lava. A thicker crust can retain more lava and increases the hydrostatic head of the flow front causing greater vertical displacement. The hydrostatic pressure is evenly distributed through the liquid lava core, which allows for a uniform uplift of the crust (Hon et al., 1994). The flows advance due to outbreaks and inflation of newly crusted lobes.

A viscoelastic layer forms between the brittle crust and the liquid core. The viscoelastic layer is stretchier than the brittle upper crust, and its tensile strength and ability to slow the flow of the liquid lava increases as it cools (Hoblitt et al., 2012). The viscoelastic layer causes lava to back-up in the conduits and inner tube system, which increases the hydrostatic head of the flow.

When penetrated by downward propagating cracks, the viscoelastic layer forms spiny glassy veneer bands. If the layer breaks and the crack is able to extend into liquid lava a squeeze-up, or break-out, forms and liquid lava spills out of the lobes to form a new lobe (Hon et al., 1994).

The monoclines that bound the inflated sheet flows' upper surfaces have dips that are between 10° and 80°, usually 20-40° (Hon et al., 1994). Hon et al. (1994) suggest the angle of monoclines is due to the viscosity gradient near the edges of a single flow; low angles result from a gradual gradient and steep angles result from sharp transitions between liquid core and viscous margin.

Cracks

Uplift of the crust causes cracks to form across the surface of a flow (Hon et al., 1994). Deep cracks around the margins are curviplanar at depth (Nichols, 1939). Inside cracks there are bands of glassy and crystalline textures thought to record brittle and ductile fracturing events, rather than de-gassing or squeeze-out events (Hon et al., 1994). Inflated sheet flows can be bounded by vertical uplift scarps, "lava-inflation clefts", which have a long wide crack running down the center of them (Hon et al., 1994). They form when the insulted liquid interior detaches from the margins and is unable to reattach. Inflation pits are formed when lava forms vertical inflation scarps around a local high area that may only have a thin layer of flow, or no covering at all.

Inflation Plateau Features

The existence of tumuli, lava rise plateaus, pits and sutures indicate endogenous growth, a process stemming entirely from inside the flow, and lava inflation (Thordarson and Self, 1998). Sutures consist of interleaved subhorizontal lava plates that connect coherent lava on either side; the suture zone plates are thickest in the middle (Thordarson and Self, 1998). A relationship exists between the subhorizontal cracks on suture zones and the lobe's vertical extension. The basal crust of a sheet lobe is much thinner than the upper crust. Thordarson and Self (1998) suggest this is due to the basal crust being a fixed boundary, unable to move like the upper crust. They also suggest the continuous addition of hot lava maintains a higher temperature in the basal crust that in the

upper crust, thereby preventing a thicker growth of cooled lower lava compared to the upper crust.

Flood Basalts

Flood basalts are large igneous provinces; these features have volumes greater than 175,000km^3 (Marshak, 2012). The Columbia River Plateau, located in Washington and Oregon, is a flood basalt that formed 15 million years ago and has a maximum thickness of 3.5 km. The Ginkgo flow of the Columbia River Basalt group is 500km long and ends in the Pacific Ocean (Ho and Cashman, 1997). The most common suggestion for the emplacement of these large volume flows is high eruption rates. Recent understanding of the inflation process has generated a different idea; flood basalts may have gradually been emplaced by endogenous processes over a longer time period, years to decades (Thordarson and Self, 1998). These endogenous processes include insulated lava transport and inflation. A 20-50cm thick lobe can inflate to a thickness of many meters thick in the space of a few weeks (Self et al., 1998). The flood basalt flows may have been emplaced in thin sheets that later inflated to greater thicknesses (Hon et al., 1994). Liquid lava is insulated within the inflated sheet and is able to be kept at extremely elevated temperatures. The theory of flood basalts' formation being due to high eruption rates, results from features formed by the maintenance of the lava's internal elevated temperatures.

The McCartys

The 3900 year old inflated McCartys flow, part of the Zuni-Bandera Volcanic field in New Mexico, is a basaltic flow with predominantly pahoehoe textures (Nichols 1946; Dunbar and Phillips 2004.). The Zuni-Bandera Volcanic Field is late-Neogene; it is bordered by the Colorado Plateau and the Rio Grande Rift (Figure 8). The Zuni-Bandera Volcanic Field consists of both alkali and tholeiitic lava flows (Peters et al., 2008). The eruption of the Zuni-Bandera Volcanic Field over the last 1.5 Ma is thought to be the result of late Neogene extension on the Rio Grande rift, the production of the Jemez lineament by crustal shearing, and rotation of the Colorado Plateau (Peters et al., 2008).

The source of the McCartys flow is a low shield volcano in the southern part of the El Malpais National Monument. The flow extends over 40 km northwards downslope towards Interstate 40 and 10km southwards (upslope) as an inflation plateau, a relatively flat-topped plateau that was uplifted by the injection of lava underneath its crust (Nichols 1946; Dunbar and Phillips 2004; Figure 9). The upper crust is a brittle layer of a flow, which also contains the highest percentage of vesicles. The core of the flow is nearly devoid of vesicles and does not have the flow textures visible on the crust. The edge of the plateau has steep escarpments, several meters high, marked by either a sub-horizontal cleft or a tilted crust (Figure 10).

The McCartys flow is composed of tholeiitic basalt, specifically quartz-normative tholeiite with plagioclase phenocrysts near the vent, within 4km, and

olivine-normative tholeiite with olivine phenocrysts further away from the vent (Renault, 1970; Carden and Laughlin, 1974).

A prominent feature of the McCartys flow is the pits that dot the distal parts of the flow towards the south and north of the source vent. Nichols (1946), who surveyed the flow from 1933 to 1935 and again in 1938, suggested that these pits formed by the partial collapse of the roof of large lava tubes. Walker (1991) calls these pits lava-rise pits or subsidence pits. Champion and Greeley (1977) were unable to find evidence of lava tubes, but Walker (1991) proposes his own theory of how subsidence pits form. He suggests the pits form when the lava inflates due to lava injection and then part of it collapses. An alternative explanation for pit formation is that an object blocks the lava flow and the lava flow inflates around the obstruction leaving a pit (Personal Communication, Andy deWet, 2013). Most workers accept both explanations as equally valid because no one has identified what factors would be useful to discriminate between the two explanations (Personal Communication, Andy deWet, 2013).

Two types of cracks occur on the McCartys flow: long, wide and deep wedge-shaped cracks, all on the scale of meters and smaller cracks that are roughly parallel to the escarpments, or edges, of the flow (Nichols, 1946). The parallel escarpment cracks are saw-toothed in places, which Nichols (1946) attributes to breaking along columnar joints. He suggests the large wedge-shaped cracks are mainly caused by the uplift of the crust during inflation, while the smaller escarpment cracks were caused by thermal contraction.

Purpose of Study

The purpose of this study is to define and provide formal descriptions of the three types of escarpment (Types A, B and C) and to apply the escarpment types to inflation plateaus identified by other researchers on Mars. The first escarpment type, Type A, has a linear slope, linear trace and one wide crack at the top of the escarpment. The second escarpment type, Type B, has a slope that is convex in some places and concave in others, a concave trace and many narrow, subparallel cracks. The third escarpment type, Type C, has a convex slope, a convex trace, and polygonally intersecting cracks.

METHODS

Field Surveying and GPS

I completed field surveying of escarpment morphology, plateau surface morphology, and crack geometry in the McCarty's flow during summer 2013, as part of a Keck Geology project supervised by Andrew DeWet (Franklin and Marshall College), Jacob Bleacher (NASA), Brent Garry (NASA), and Chris Hamilton (NASA). On escarpments, neighboring plateaus and floor surfaces, I made measurements of surface inclinations and shapes using a Brunton compass and a Trimble Differential Geographic Positioning System (DGPS) with +/-2-4cm vertical and horizontal precision.

I gathered data about various escarpments on the southeastern lobe of the McCartys, specifically 1-2 slopes typifying each escarpment type. With a measuring tape as a guide, we marked a straight line every meter with a tin foil covered rock, in order to maintain a straight traverse. We first made traverses of the foil-covered rock lines using the DGPS device to measure locations along the traverse, and a Brunton compass to measure escarpment surface inclination at approximately one meter increments in order to measure escarpment shapes and slope change on the three escarpments. We photographed all three slopes in detail.

I also used the DGPS to map transects parallel to the trace of the escarpments and on the relatively flat plateau surfaces. We completed several traverses across a horseshoe shaped inflation pit. The rocks for the traverses were laid down every few meters and within sight of the previous rock in a straight

line. Some of these traverses cut across the horseshoe and ran around its margins. We measured two traverses across the relatively flat inflation plateau top, one traverse intersected three large inflation pits and the other did not cross any pits. The pits in the inflation plateau were observed, described and sketched. Most of the smaller pits were about ten meters wide and partially filled with rubble. For each crack in the escarpment or plateau surface we crossed during a traverse, we took width and depth measurements at the point of crossing. We imported the DGPS data into excel sheets and then transferred it into ArcGIS.

GIS

Using air photos (the ArcGIS basemap called World Imagery), I used ArcGIS to map and categorize the cracks along the escarpments of other parts of the southeastern part of the McCartys flow (i.e. parts not studied in the field). ArcGIS' basemap has a one meter or better precision and is composed of a combination of satellite and aerial imagery. The cracks on the escarpments were highlighted using magenta lines and the edges of the inflation escarpments are outlined with yellow lines. With the aid of the crack patterns on the escarpments, I covered various sections along the inflation plateau with either a yellow polygon symbolizing Type A crack patterns, a blue polygon symbolizing Type B crack patterns, or a pink polygon symbolizing Type C crack patterns. I used green polygons to mark zones of transitions between crack pattern types, or zones that I was unable to categorize. Zones can be difficult or impossible to categorize for a variety of reasons including: a poor satellite angle, a large pile of debris obscuring

the cracks, and evidence of secondary inflation or flow overriding the primary inflation seen in the surrounding escarpments.

Analysis of the satellite images of escarpments that I studied in the field could have be biased by my field observations. In order to remove this bias I turned off the satellite and zone identification layers, and then re-evaluated the zone identifications using only the magenta crack lines and yellow inflation plateau outlines.

RESULTS

Escarpment Type Overview

Using the mapped features and DGPS data, I identified and defined three types of escarpments based on their slope shape, traverse shape and crack qualities. Type A escarpments have linear slope, linear traces and one wide, 2-3m, crack along the top of the slope. Type B escarpments have slightly convex slopes, concave traces and many narrow, less than 1m wide, sub-parallel cracks. Type C escarpments have convex slopes, convex traces and cracks of various widths that intersect at many different angles.

DGPS Traverse Data

Type A

Traverse J is an excellent example of the Type A morphology of the escarpment (Figure 11). The graph of the DGPS points for Traverse J shows the edge of the escarpment has an overall liner slope. Traverse J has four cracks, the one at the top of the slope is 2.5 meters wide, and none of the other cracks is wider than a meter. The two measurements on top of the plateau have a slope of 0° and 5°, these are the most horizontal slopes (Figure 11). Most of the slope measurements are between 19° and 39°. Most of this section of slope measurements average 30°, giving this escarpment an overall linear slope. The three slope measurements at the bottom of the slope are between 56° and 65°. This extremely steep slope is a local anomaly that appears to be due to a slab that had slipped down and was surrounded by rubble.

I made a 10 meter traverse of the trace of the escarpment, 5 meters north and 5 meters south of the bottom of Traverse J (Figure 12). The two northernmost inclination measurements were 10° and 17°; however, both were taken around a rubble pile and are therefore discounted. The eight other inclination measurements varied between 0° and 3°, indicating the trace of this Type A is relatively linear.

Traverse B displays two cracks, the wider crack is on the escarpment and the narrower one is on top of the plateau (Figure 13). The crack on the escarpment is approximately 2 meters wide. The escarpment has a linear shape (rather than curved) with a 45° slope inclination and a height of 14 meters.

Both Traverse J and Traverse B have similar crack depths and geometries (Figure 14). Traverse B's two cracks have very similar depth, 7.25m and 7m. The wider upper crack is the slightly deeper one. Traverse J's widest crack, 2.2m, is also the deepest at 6.2m. The lowest crack on the slope is 1m wide, but the shallowest at 2.1m. The two cracks between the small bottom crack and largest crack at the top of the slope are almost identical in dimension, one is .64m wide and 3.2 deep and the other is .65m and 3.3m deep.

In summary, Type A escarpment morphology is characterized by a linear slope, linear trace and one large, wide, crack near the rim, other cracks are smaller and parallel to the larger crack.

Type B

Traverse K is an example of the Type B morphology of the escarpment (Figure 15). The graph of the DGPS points for Traverse K demonstrates the letter 'S' appearance of the slope. The 'S' is created by local variations in plate positions. Plates on the slopes are sections of escarpment bounded by cracks. Individual plates have the same slope; however, the slope of the escarpment is not uniform. The slope of Traverse K is non-linear: it is concave near the bottom of the slope, the linear in the middle and convex near the top. The steepness of the slope appears to generally decrease from bottom to top. The bottom two thirds of the escarpment has slope measurements between 30° and 55°, the upper part of the slope shows a steady decrease from 40° to 10°. There is a local steepness reversal near the top of the slope before reaching the horizontal 0° plateau top. Traverse K has 10 cracks, these cracks are rarely, if ever, wider than one meter, and are subparallel to each other. Traverse L is along the trace of the same escarpment (Figure 16). The trace of this escarpment is concave.

Traverse F has four narrow cracks marked on the slope and three more on the plateau top (Figure 17). None of these cracks are wider than half a meter. The bottom of the slope has a somewhat concave and horizontal slope before becoming more convex and curving into the horizontal plateau top.

The cracks Traverse K and Traverse F cross, fall within a similar range of depth (Figure 18). The seven cracks along Traverse F are all less than .6m wide, but the crack depths are less consistent in size (Figure 18). The lowest crack on

the slope is the shallowest at .35m deep. Of the three cracks near the top two are 4.3m deep, the deepest depth recorded for this slope, and one was too full of rubble to measure an accurate depth. The eleven cracks along Traverse K have depths ranging from 0.69m to 4.25m (Figure 18). The depths deeper than 1m tend to be on the upper part of the slope. There is no apparent relationship between depth and width on this slope.

In summary, Type B escarpment morphology is characterized by an 'S'-shaped slope, concave trace and lots of similarly sized small, thin, cracks subparallel to each other.

Type C

Traverse M is an excellent example of the Type C morphology of the escarpment (Figure 19). The graph of the DGPS points for Traverse M shows the edge of the escarpment has an overall convex slope. The three cracks crossed by Traverse M vary in width from .3 meters to 1.1 meters wide. The escarpment appears to be divided into three separate sections of slope steepness. The bottom of the escarpment is the steepest, ranging from 36° to 45°, the middle section ranges from 15° to 33°, and the top of the escarpment ranges from 8° to 14°.

Part of Traverse M is along the trace of the escarpment on which another part of Traverse M crossed a Type C escarpment (Figure 20). The traverse is a convex semicircle, consistent with the idea that Type C escarpments have convex traces.

Traverse D shows a slightly convex slope (Figure 21). There are three cracks marked on the traverse: one is .55m wide, and the two further up the escarpment are 2.65 and 1.65m wide. The two wider cracks are also much deeper, more than 6m, than the narrow crack.

Traverse M and Traverse D contained the deepest cracks found on any of the escarpments. Traverse M crossed three cracks ranging from .7m to 1m deep (Figure 14). Traverse D crossed two cracks: the wider one is 2.65m wide and 7.96m deep and the narrower one is .55m and 3.09 deep (Figure 22). Traverse D's wider crack is, at 7.96m, the deepest crack measured during the field study.

In summary, Type C escarpment morphology is characterized by a convex slope, convex trace and many polygonal, intersecting cracks of various widths.

INTERPRETATIONS

Type A Data Interpretations

The uniform slope of the Type A escarpments is consistent with the idea of their creation by plateau uplift. Type A escarpments have fairly uniform slopes, with only limited local inclination outliers. Analysis of the compass measurements of the trace of Traverse J's escarpment match up with the visual observations to confirm that it does in fact have a fairly straight, linear, trace. When a simple uplift of a plateau occurs, the margins of the flow crack under the stress. If the amount of liquid lava uplifting the plateau maintains a constant pressure, the escarpments should have a triangular geometry. Type A slopes can have several sub-parallel cracks, but one is always significantly wider than the rest. It is this wide crack that forms the hinge between the top of the plateau and the escarpment. All the cracks are very deep; the wider cracks are typically deeper. The larger cracks are created by higher stress levels, so the widest and deepest cracks are located at the point between the escarpment, a point of inflation uplift failure, and the horizontal plateau.

Type B Data Interpretations

The simple uplift model for the Type A escarpments does not seem to fit the Type B escarpments; instead, Type B escarpments appear to be created by local deflation during the uplift process. Type B escarpments do not have linear inclinations, the escarpments are composed of convex and concave inclinations. Type B escarpments lack the perfect triangular geometry of Type A escarpments.

The concave trace shape also supports the idea that the pahoehoe sheet was not simply vertical translated. The concave trace suggests a collapse of the escarpment into the plateau. None of the cracks on the Type B escarpments are as wide or deep as those found on Type A escarpments, but Type B has more cracks. The cracks are the physical remnants of the stresses felt by the escarpments. The way stress is spread across the escarpment during plateau uplift is not the same as the stress distribution across a Type A escarpment. It is likely that there is a disruption during the process of uplift. The increased number of cracks are a product of this disruption because the stress is not concentrated at the top of the escarpment, the point of initial failure. Instead the disruption in uplift, a local decrease in liquid lava under the brittle crust, caused a local deflation.

Type C Data Interpretations

Type C escarpments are created by a combination of plateau uplift and a local excess of liquid lava in the core. The convex inclination of Type C escarpments does not fit with a simple plateau uplift because the escarpment is not only uplifted, but pushed out from the plateau as well. The convex trace supports this interpretation as well because these aspects combined show that the escarpment has been pushed out in all directions. This idea fits with the polygonal appearance of the cracks, which can be interpreted as being due to stresses acting in several directions on the escarpment.

Overall DGPS Data Interpretations

The depths of the cracks on Type A are the deepest of the three escarpment types because they are caused by crust failure (i.e. the basalt crust literally tore during the inflation process). Type B cracks are the shallowest and appear to be caused by deflation. Deflation causes the crust to sink into the plateau, but it does not involve the same extreme stress as inflation. Type C crack depths measured on the traverses ranged from very deep to very shallow, which could be explained by the inaccuracies of measuring the polygonal crack patterns with a straight line. The variable crack depths could also be related directly to the over-inflation process that forms Type C escarpments. The cracks at the top of the slope are slightly deeper than the other cracks on the slope, in both Traverse D and M, because the top of the escarpment experiences the largest amount of stress and failure as happens with Type A escarpments.

I applied the three escarpment definitions to escarpments across other parts of the McCartys flow using satellite imagery (Figure 23; Figure 24; Figure 25). Type A escarpments are the least common of the three in these areas because the flow tends to have rounded edges rather than long linear escarpments. Type A escarpments most likely require a smooth topography to form because the flow is then able to form a smooth upper layer and not flow around objects to create rounded flow edges. (Self et al., 1998).

Escarpment sections that do not fit into any of the escarpment type definitions are created by processes other than uplift of the plateau. A downward

propagating crack on an escarpment can pierce the viscoelastic layer and create a breakout that will flow out over the escarpment and have a relatively smooth and crack-free surface, at the same time it obliterates the previous surface (Crown and Baloga, 1999; Hon et al., 1994). Other sections may be rubble and crack-filled suture zones between breakouts and escarpments types.

DISCUSSION

All previous workers on the McCartys flow and on other inflation plateaus agree that escarpments form during inflation (Hon et al., 1994; Walker, 1991; Self et al., 1998; Hoblitt, 2012). No previous workers have distinguished between different escarpment geometries. The results represented here distinguish three distinct escarpment geometries: Type A (a linear or straight slope of 30-45 degrees with a linear trace), Type B (a non-linear slope with a concave trace), and Type C (a convex slope with a convex trace). Furthermore, each type displays distinctive crack geometries perhaps due to varying rates of plateau growth (i.e. magma injection) and local deflation phenomena. Although this study is the first to document these three escarpment geometries, previous workers have interpreted other variations in escarpment geometry in terms of local topographic variations and obstacles to lava sheet flow.

Inflation Process

Type A and C escarpments are created by the uplift of the plateau during inflation. When the brittle crust is uplifted by the injection of liquid lava the material is only able to deform plastically, before it breaks under the stress of being uplifted (Figure 26). Hoblitt et al. (2012) describes how once a failure has developed in the brittle and viscoelastic crust due to cooling-induced shrinkage, or additional liquid lava input, the failure persists and the flow will continue to crack along that line as the sheet flow inflates. The cracks are the representation of the stress and if the cracks were to close the plateau would drop to the height of the

pre-inflated sheet flow (Figure 26). It is easy to see this theoretical reversal process working on Type A escarpments, but it is not possible with Type B and C escarpments because they do not have linear slopes. Type C escarpments have a swollen appearance due to their convex traces and slopes; their appearance is tied to the formation of Type B escarpments.

Deflation/Collapse

Type B escarpments are created by localized deflation or collapse of an escarpment during the uplift of an inflation plateau. The cracks on a Type B escarpment look like the cracks that form on a cake that deflates as it cools. Walker (1991) explained that some tumuli are caused by the irregular collapse of the lava crust due to the drainage of underlying fluid lava. Tumuli are inflated volcanic features similar to inflation plateaus and are therefore subject to the same processes. Type B escarpments do not have perfect linear slopes and the associated trace is concave, so it does not fit the ideal uplift model presented in Figure 26. The liquid lava moves from behind Type B escarpments to behind Type C escarpments through the sub-brittle layer conduits, described by Hon et al. (1994). The movement of the liquid lava in this fashion causes the Type B escarpments to partially deflate and the Type C escarpments to swell with excess lava.

Topography and Obstacles

Inflation, deflation and collapse are not the only processes that can control the shape of an escarpment. Topography and the presence of obstacles impact

tumuli formation and lava flow geometry (Walker, 1991; Hon et al., 1994; Self et al., 1998). Objects that are not initially covered by a pahoehoe flow can be partially buried or, passively surrounded and later uplifted during the inflation process (Hon et al., 1994). This means that a topographic feature or obstacle can have an impact on the shape of a lobe while it is still plastic and inflating, and then be obscured later on. The importance of topography or obstacles as the cause of escarpment shapes has not been determined. At the McCartys flow the traces of all escarpments examined during summer 2013, were covered by rubble or lava flows post-uplift. This made original topography and obstacles impossible to determine.

Additional Data Needed

We did not collect the data sets necessary to test the hypothesis that Type B escarpments formed by deflation. In order to test this hypothesis, DGPS traverses are needed with corresponding crack widths and depths for several neighboring Type B and Type C escarpments. These data could show that a Type B escarpment, when collapsed back down vertically, has a horizontal displacement equal to the Type C escarpment next to it. When a Type C is bordered by two Type B escarpments, or vice versa, the displacement should be spread between the three escarpments. Therefore, this hypothesis is best tested by pairs of Type Cs and Bs, bordered by Type A escarpments. When cracks on Type A escarpments are theoretically closed, the plateau would drop back down to the original height of the sheet flow, and the displacement would be approximately

zero (Figure 26). My hypothesis predicts that closing the cracks in Type B and C escarpments would not create displacements of zero.

Mars Inflation Plateaus

It is possible to map cracks and margin shapes on Mars using satellite imagery, or to get an idea of the slope of an escarpment using satellite elevation data (although I did not have satellite elevation data for my study). Here, I apply my escarpment type definitions to the escarpments on inflation plateaus identified by Keszthelyi et al. (2008), Hamilton (2013), deWet (Personal Communication, 2014).

Keszthelyi et al. (2008) identify and discuss an inflation plateau on Elysium Planitia (Figures 2 and 27). The volcanic feature they identify as an inflation plateau is uplifted above the surrounding Martian terrain. The southwestern part of the image is entirely uninflated. The northeastern part of the image shows small sections of inflation, but nothing appears to be as tall, or on the same scale as the inflation plateau running diagonally though the image. I located the HiRISE imagery for this plateau in order to get a closer look at the escarpments (Figure 28). I cannot see cracks on the feature, so I am unable to identify any escarpment types. The inflation plateau is either too small, or the image is of insufficient resolution, or the dust covering is too thick. This feature should have cracks if it is an inflation plateau because cracks are a sign of the inflation process breaking the brittle upper crust (Hon et al., 1994).

Hamilton (2013) identify an inflation plateau, which is part of the Cerberus Fossae 2 unit northeastern Elysium Planitia (Figure 3). The escarpment shown in the zoomed in image has several wide subparallel cracks, which Hamilton refers to as inflation clefts (Figure 3b). The relatively smooth section of terrain in the southwestern corner of the image is uninflated. The margin of the escarpments are bending shadows between the uninflated material and inflated flow. In the northwestern corner of the image the escarpment curves slightly. The cracks in this area are not as visible as the areas on either side of the curve. I identified a Type A escarpment (southeast), a suture zone (the curve) and another Type A escarpment (northwest). In general, Type A escarpments have a wide crack at the top, with some narrower subparallel cracks on the escarpment or up on top of the plateau. Both the identified Type A escarpments in the image have one distinctive crack visible at the top of the slope. Without satellite elevation data I am unable to tell if the slope is linear. Although, the trace of both Type A escarpments is not particularly linear, the cracks, which are always subparallel to the top of the escarpment, are linear. Hamilton (2013) grouped the zoomed image (Figure 3b) with a regional image (Figure 3a) and an inflation escarpment from the McCartys flow (Figure 3c). I examined the escarpment in Figure 3c and identified it as a Type A escarpment. I agree with Hamilton's use of this McCartys flow escarpment as a terrestrial analogy, because the Martian escarpment (Figure 3b) is composed of two Type A escarpments.

DeWet (Personal Communication, 2013) also identified an inflation plateau in Elysium Planitia (Figure 29; Figure 30). The margins of the inflation plateau certainly appear to show some escarpment type characteristics. The top of the inflated plateau is clearly uplifted above the material to the east of the image. When examining this image I found that the traces of the escarpments and the edge of the uplifted material were not in the same place. The steep escarpments, whose traces I outlined in yellow, create a shadow on the material below; however, the slightly uplifted material at the foot of the escarpments does not cast a shadow. I identified all three escarpments on the margin of this section of the inflation plateau (Figure 29). The escarpment outlined in blue is a Type B escarpment because it has a concave trace and several subparallel cracks. The escarpment highlighted in pink and green boxes is most likely a Type C escarpment, it has a convex trace and what appears to be cracks in several directions. The escarpment highlighted with yellow and green checkers is a Type A escarpment because it has a linear trace and a few wide cracks. My identification of all three escarpment types allows me to agree with deWet's original identification of this feature as an inflation plateau.

DeWet (Personal Communication, 2013) also identified another uplifted escarpment as part of an inflation plateau (Figure 31). Although the feature (Figure 31) is clearly uplifted above its surrounding terrain, I am not convinced it is the escarpment of an inflation plateau. I highlighted the cracks on the figure with magenta lines and noticed that they run subparallel to the curve of the

feature. There are many narrow, subparallel cracks that run down the center of the feature, instead of on one of the slopes, so this is not a Type B escarpment. There is no plateau connected to either side of this feature; instead it appears to be a standalone feature. If it is a volcanic feature, then it is probably a pressure ridge because the cracks look like axial clefts. Pressure ridges are essentially elongated tumuli (Wentworth and Macdonald, 1953).

Elevated plateaus on Mars are not necessarily inflation plateaus. Keszthelyi et al. (2008) proposed the interpretation of pingos for one identified feature, which they later dismissed on the grounds that the edge of the feature ended too abruptly. Large features with cracks that look like inflation plateau escarpments could instead be glacial features, particularly above latitude 30°N and below latitude 30°S. Tanaka (2005) mentions that glacial moraines and kame complexes are common interpretations of Mars features without clear terrestrial analogs. Both of these features can be several hundred square kilometers on Mars and appear to be crack covered escarpments or inflation pits. The best place to locate inflation plateaus is on the plains of Elysium near the large shield volcanoes and not in the glacial zones.

CONCLUSIONS

In the summer of 2013 I conducted fieldwork on the McCartys flow, in New Mexico, with the aim of using it as analog for inflation plateaus on Mars. The McCartys flow is relatively young, 3900 years old, and unweathered, so it gives a good picture of a freshly formed inflation plateau (Nichols, 1946). I identified and defined three types of escarpments on the McCartys flow. The three escarpment types are products of different processes related to the uplift of the plateau. The first type, Type A, is the simplest of the three escarpment types because it is directly created by the failure of the pahoehoe lava under the stress of inflation and plateau uplift. The second and third types, Types B and C, are created by the movement of liquid lava inside the pahoehoe sheets during uplift.

With the advent of HiRISE imagery, researchers have interpreted several volcanic features on Mars to be inflation plateaus. The three escarpment types can be identified using satellite data. Identification of the three escarpment types on a Mars feature adds to the evidence that the feature is an inflation plateau. It also gives hints about the local volcanic history during plateau uplift. Using the escarpment type definitions, I was able to confirm the identification by other researchers of at least two of volcanic features on Mars as inflation plateaus.

ADDITIONAL WORK APPENDIX

PEG wax Analog Modeling

Polyethylene glycol 600 (PEG wax) is a wax that when cooled from a liquid to a solid state displays rheology similar to a lava flow and has been used to model lava flow behavior before (Fink and Griffiths, 1990; Gregg and Fink, 2000; Balmforth, 2000; Blake and Bruno, 2000; Garry et al., 2007; Applegarth, 2009). I used the wax to model lava behavior and crack formation on the edge of an inflation plateau. Inflation plateaus are impossible to accurately model by including all aspects (Glaze and Baloga, 2013); therefore this model only focuses on lava, or wax, inflating and cracking on the edges.

Methods

The five PEG wax trials were conducted using a fish tank, 9 inches tall, 14.5 inches long and 8 inches wide (Figure 32). A 2cm hole was cut into the bottom of a fish tank and a connector fitting was slotted into the hole. The fish tank was elevated above the bench by four notched wooden blocks, ten centimeters tall. I inserted a 1.4cm thick book between the tank and two of the supporting blocks on the side closest to the suspended vial to create a 1.98° slope. A 40cm long pipe with a diameter of 3/4cm was fitted with one end to the connector fitting and the other end to a peristalsis pump. Another identical pipe connected the other end of the peristalsis pump up to a 300ml reservoir. The glass vial reservoir was held by a rod 45cm above the level of the bottom of the tank. I filled the tank with 5 liters of sucrose solution which had been refrigerated at a

temperature of about 5ºC; this temperature is well below the solidifying point of the PEG wax. The sucrose solution had a density of 113.3 g/ml in the early analog model runs, and a slightly lower density of 111g/ml in runs 3-5. The PEG wax was heated in a microwave for 20 seconds until melted and then blue dye was added. The wax was poured into the suspended glass vial, traveled through the pipes and was pumped into the cold sucrose solution in the tank. It then flowed along the bottom of the tank before solidifying. I used a video camera and a still camera to record the movement of the wax, and a Taylor meat thermometer to measure the temperature of the wax, sucrose solution and room before each of the trials began.

PEG Wax Analog Model Analysis

Obstacles can change the internal hydrostatic pressure of the flow. During trial 5, I placed a square tin into the fish tank on the downhill side and allowed the wax to flow into it, the overall direction of wax flow changed (Figure 38). A wall of solidified wax formed up against the square tin, and remained even after the tin was removed (Figure 39). The wax was able to flow up-slope due to this build-up (Figure 40). This was most likely due to the forced even distribution of the hydrostatic pressure of liquid wax inside the flow. Conduit blocking and even distribution of hydrostatic pressure also occurs within inflated sheet flows (Hoblitt et al., 2012; Hon et al., 1994). The solidified wax wall blocked up the inner conduits and the pressure forced the wax to flow uphill. Later a new breakout

was able to form above the vent and the flow redirected downhill once more (Figure 41).

New lobes of wax can break out from underneath other lobes or from the connection between lobes. The plastic nature of the wax does not allow for the wax to break; therefore, wax is not useful for observing cracks or breakouts from cracks. The flow of wax is very susceptible to changes in direction due to obstacles in its path and solidification of its crust. Liquid wax moves underneath the solidified crust and can breakout in any part of the flow where the crust is thin or weak enough. All the wax lobes swell and have round shapes similar to pahoehoe sheet flows before the formation of the brittle upper crust (Figure 42; Hoblitt et al., 2012). Therefore the wax is a basic analog for the liquid lava inner core and the ductile viscoelastic layer, but not for inflation plateaus.

PEG Wax Runs

- During trial runs one and two, the PEG wax floated in the sucrose solution (Figure 33, 34 and 35). This was caused by the sucrose solution density being higher than the PEG wax density. The sucrose solution has to have a density of 111g/ml for the PEG wax to be able to flow along the bottom of the tank as seen in runs 3-5.
- The most effective PEG wax starting temperature is 5˚C. Warmer temperatures than 9°C and it will remain in a liquid state and never form solidified lobes (Figure 36 and 37).

- For this experiment, I used a 1.98˚ slope in order to create an artificial slope. Shallow angles work best because wax still needs to be able to flow slowly.
- PEG wax solidifies, but never becomes brittle. This means it never forms cracks and is therefore not suitable as an inflation plateau modeling material.

FIGURE APPENDIX

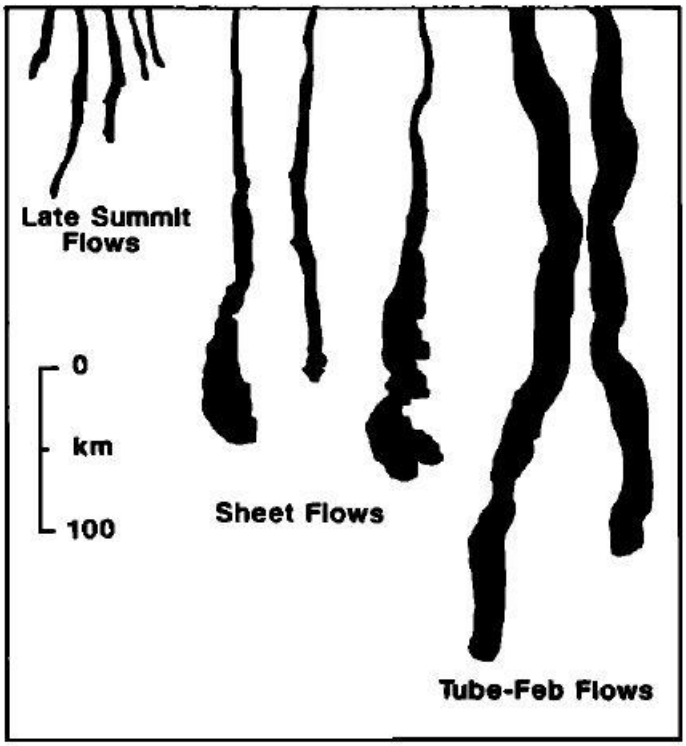

Figure 1. Morphological spectrum of lava flow types on Mars. Figure from Wilson and Head, 1994.

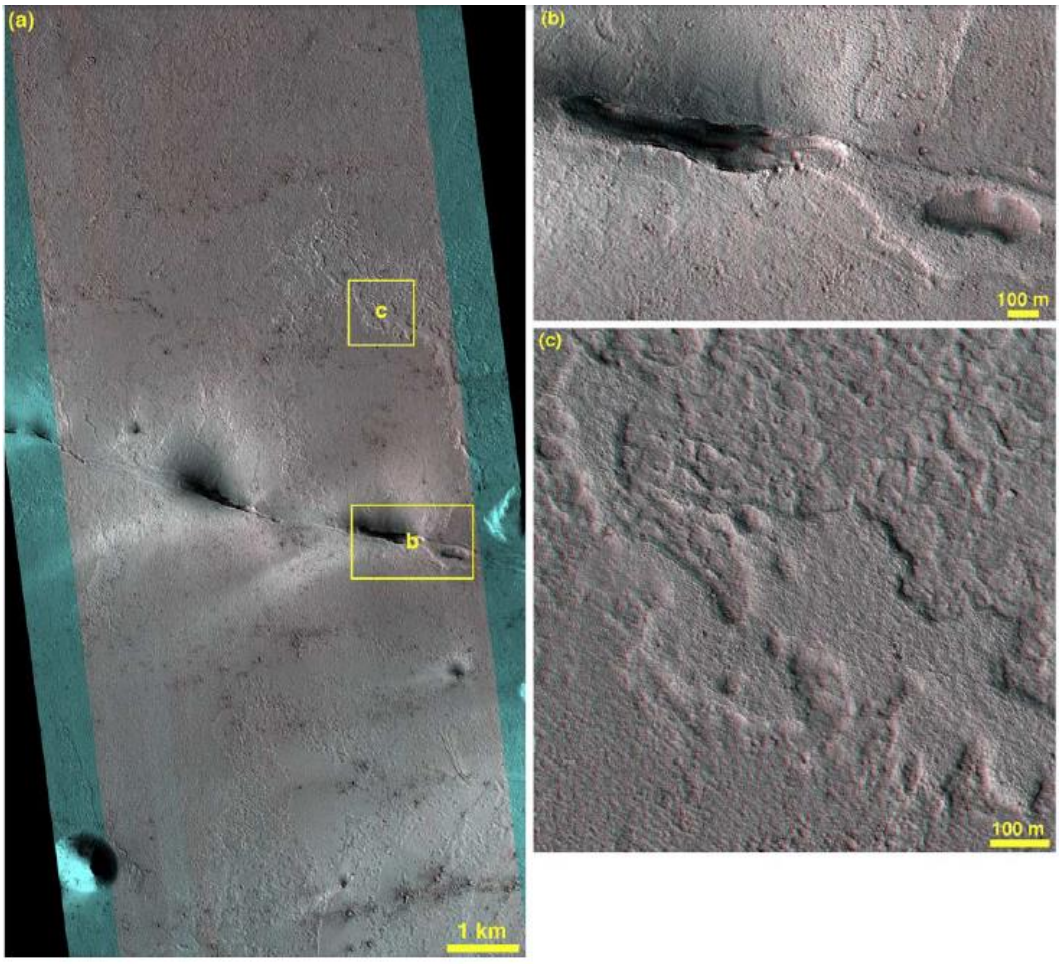

Figure 14. Inflated lava flows in Elysium Planitia. (a) Anaglyph produced from HiRISE observations PSP_003241_1880 and PSP_003531_1880. The diagonal banding is due to imperfect calibration of these hazy images. A segment of the Cerberus Fossae cross the center of the figure, but it is unclear if it was the source of these lavas. (b) Close-up centered at 7.688°N, 164.418°E showing collapsed and inflated lava over the fissure. (c) Close-up centered at 7.741°N, 164.410°E showing a classic example of an inflation plateau.

Figure 2. Adopted from Keszthelyi et al., 2008. Image C on the bottom right shows an inflation plateau on Elysium Planitia. Note the fairly flat plateau looks hummocky, suggesting an uneven terrain.

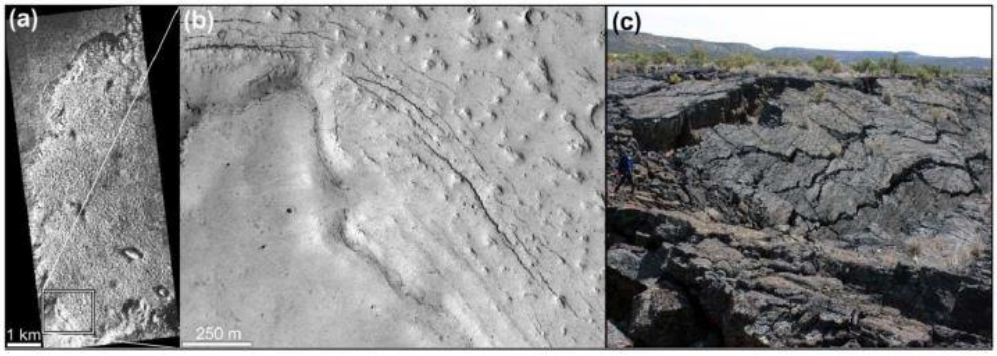

Figure 3. Figure adopted from Hamilton, 2013. (a) HiRISE ESP_018035_2080 shows part of the Cerberus Fossae 2 unit northeastern Elysium Planitia, Mars. (b) Magnified view of cracks along the margin that are interpreted to be inflation clefts in a pahoehoe-like lava flow. (c) Analogous inflation clefts near the ~15 m-high margins of the McCartys lava flow, New Mexico.

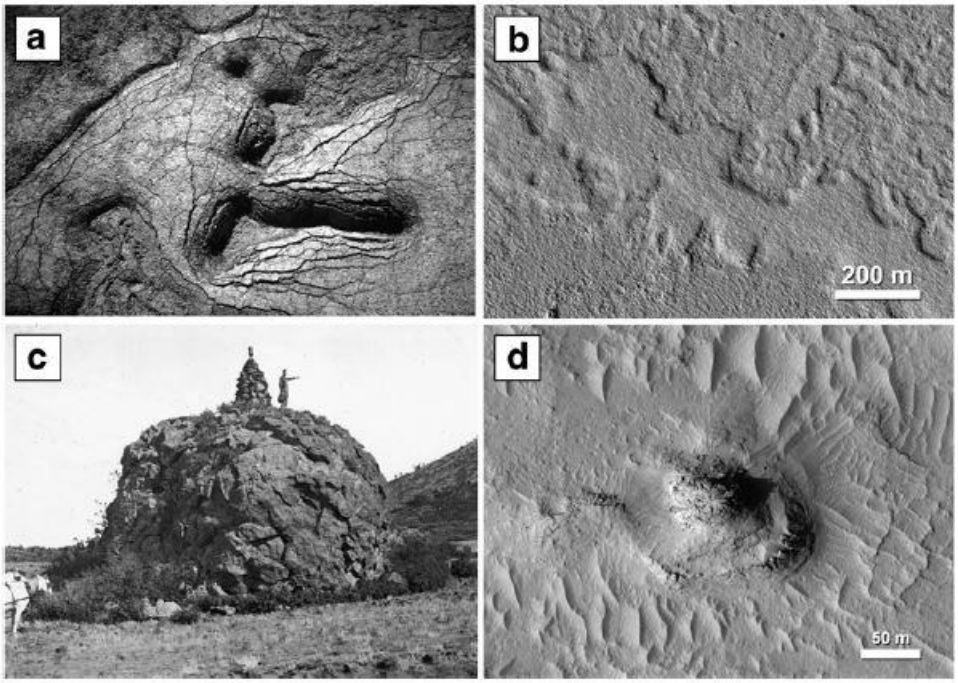

Figure 4. Figure taken from Hauber et al., 2009. (a) Lava inflation plateau with fractured surface southwest of Craters of the Moon National Monument, Snake River Plain, Idaho. (b) Lava inflation plateau in Elysium Planitia. (c)Tumulus near Capulin Volcano, New Mexico. (d) Possible tumulus on low shield in the Cerberus Plain, Mars. Hauber et al. say the bread-crust-like appearance suggests cracking of a solidified surface by injection of liquid lava.

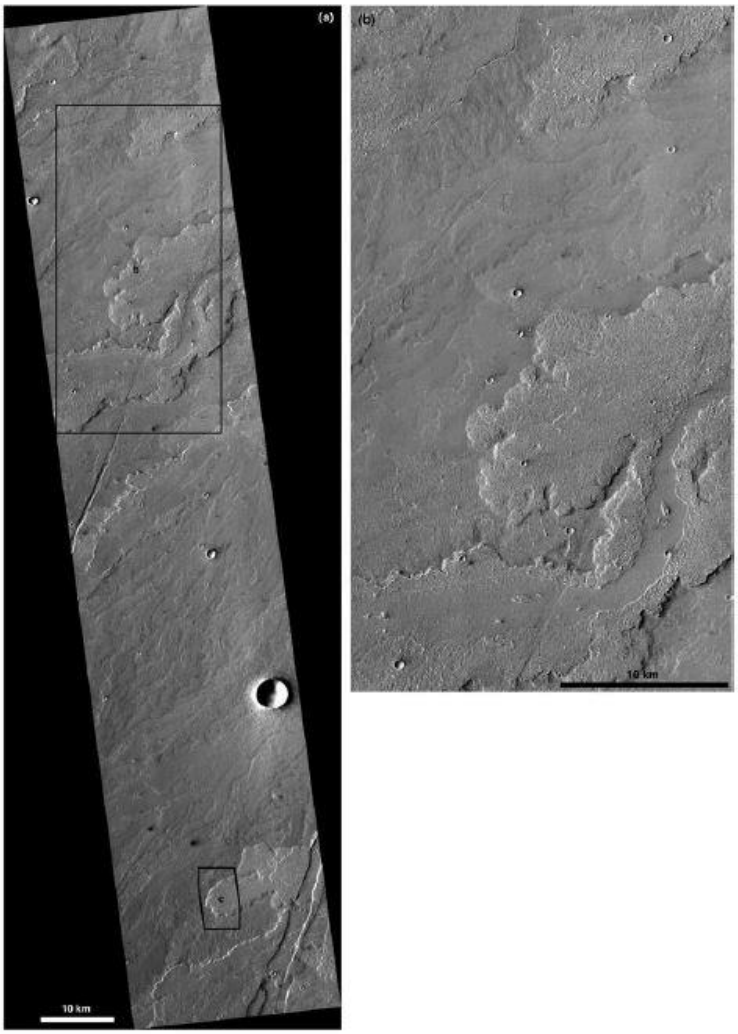

Figure 5. This figure of the lava flows of Daedalia Planum is taken from Keszthelyi et al., 2008. (a) This image shows an area overview, CTX image P04_002711_1560. (b) This image is a close up of the largest box on image A. The north contains narrow channels with many overflows, and the south contains wide channels with streamlined islands.

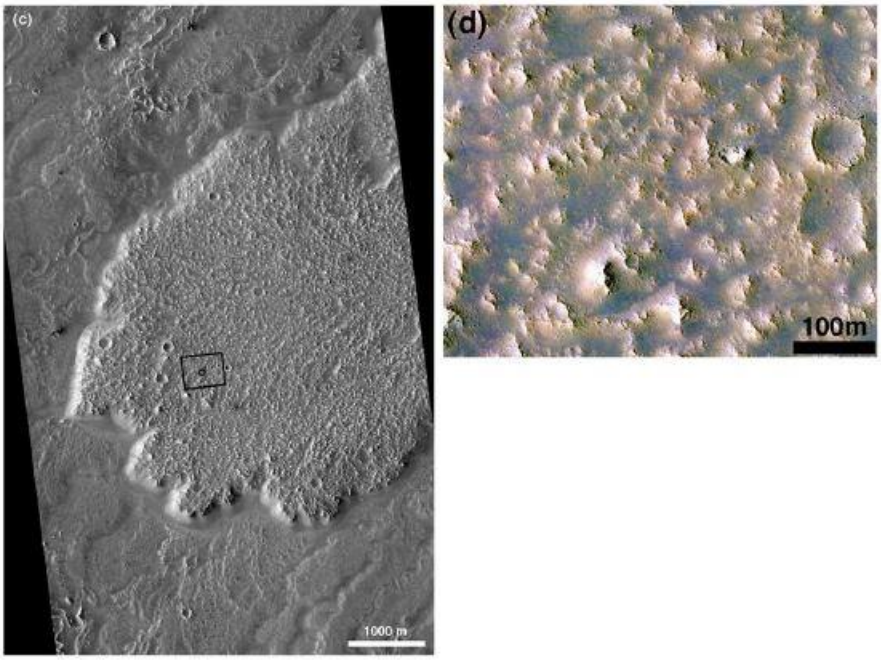

Figure 6. Lava flows of Daedalia Planum. The image on the left (c) is a close up of the smaller box on image A in figure 5. This thick lava lobe has a "ridged" brecciated top. The image on the right is a close up of the image on the left in false color. (Keszthelyi et al., 2008)

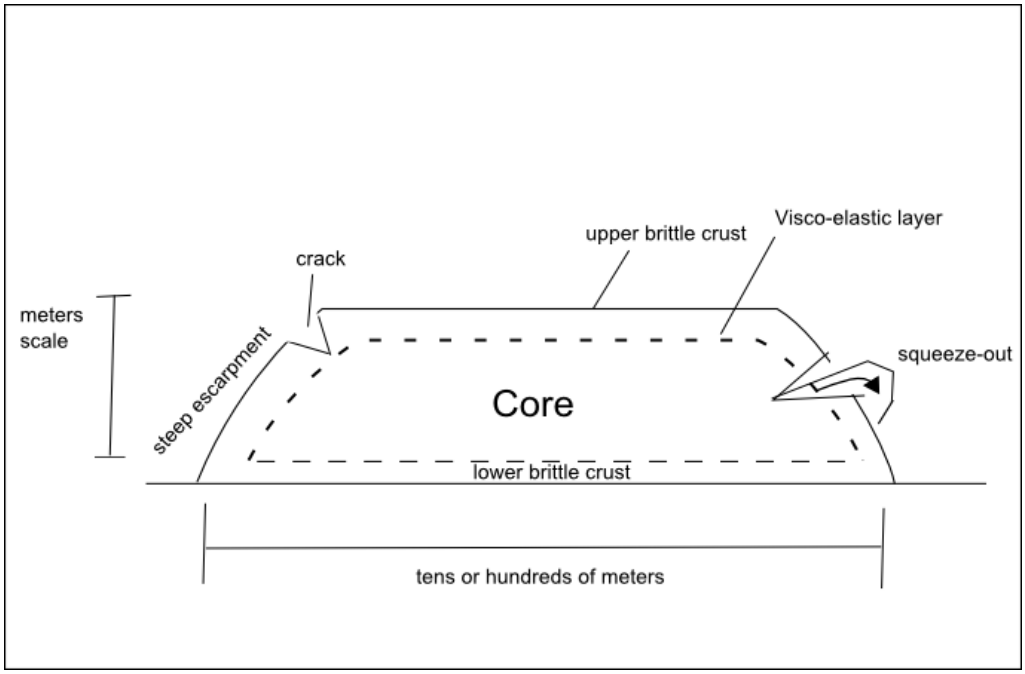

Figure 7. Cross-section of an inflation plateau. Inflation plateau are several meters tall and tens or hundreds of meters across. Note the three layers of the inflation plateau: liquid lava core, ductile viscoelastic layer and brittle upper and crusts. The brittle lower crust is thinner than the upper crust. The squeeze-out is liquid lava emerging through a crack to form a new lobes. The field work for this paper was focused on the steep escarpments of the plateau.

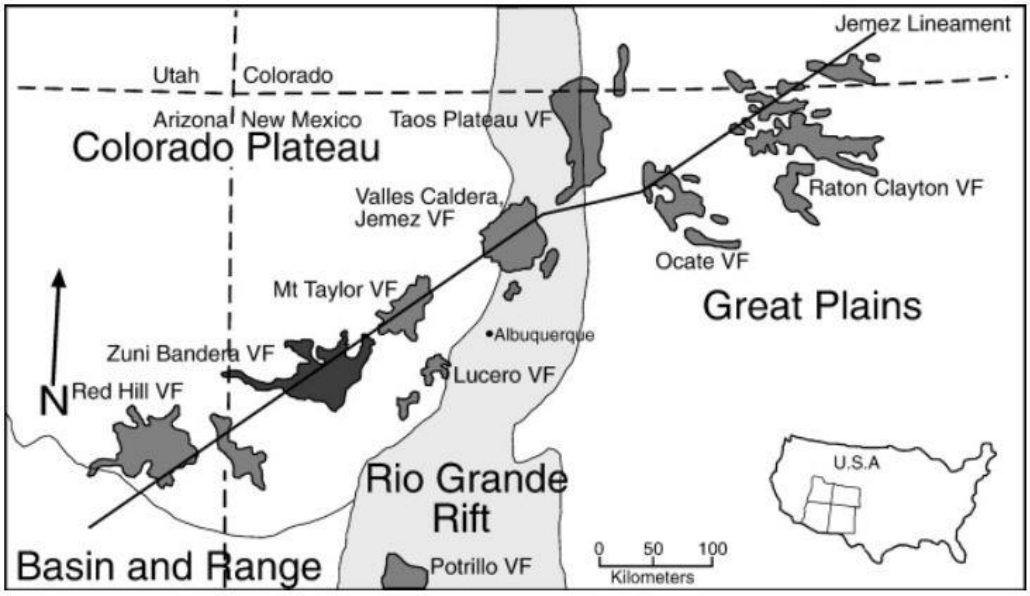

Figure 8. Map taken from Peters et al., 2008. The McCartys flow is part of the Zuni-Bandera VF. The Zuni Bandera VF lies on the Jemez lineament and to the west of the Rio Grande Rift.

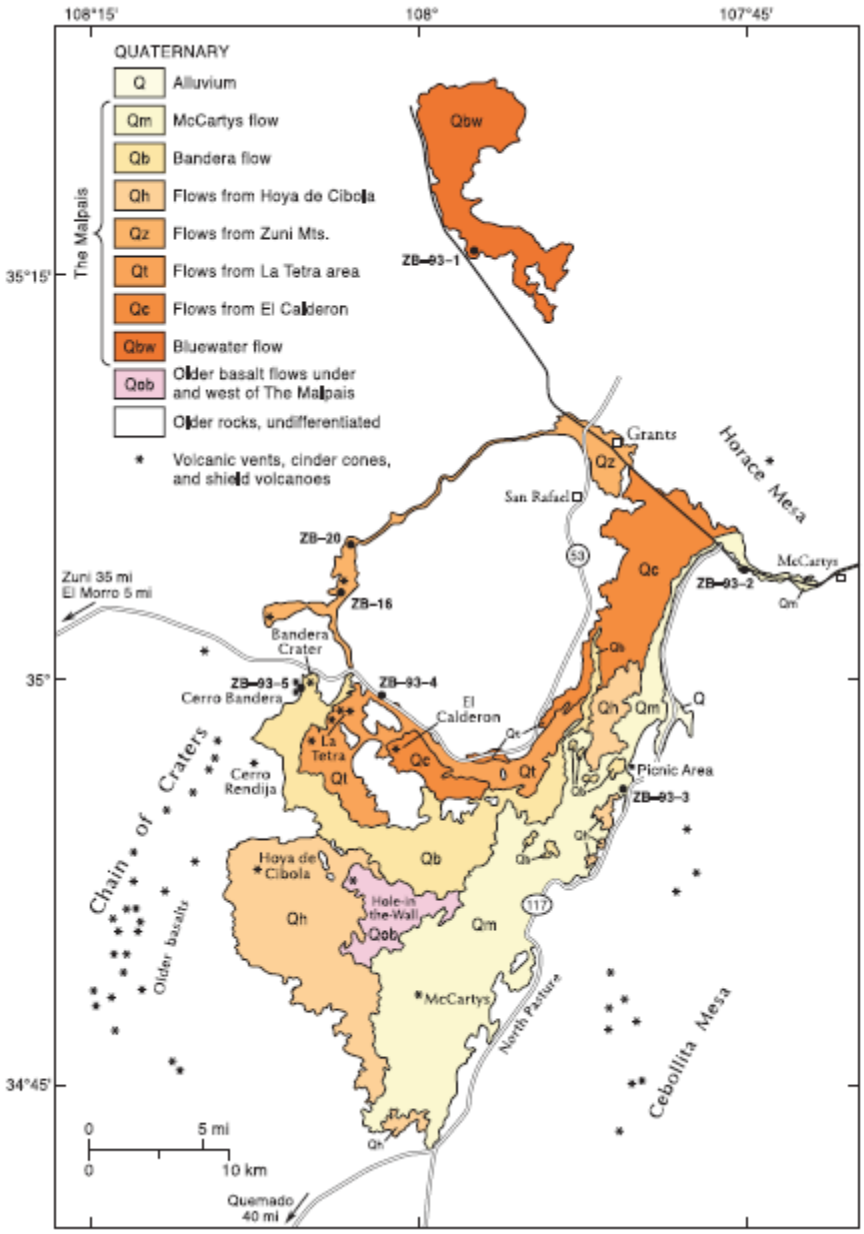

Figure 9. Adapted from Dunbar and Phillips, 2004. Note the red dot labeled McCartys is the vent location for the McCartys flow. The red box highlights the eastern tail where field research was focused.

Figure 10. A step escarpment on the McCartys inflation plateau. Note the two people standing at the top of the escarpment for scale.

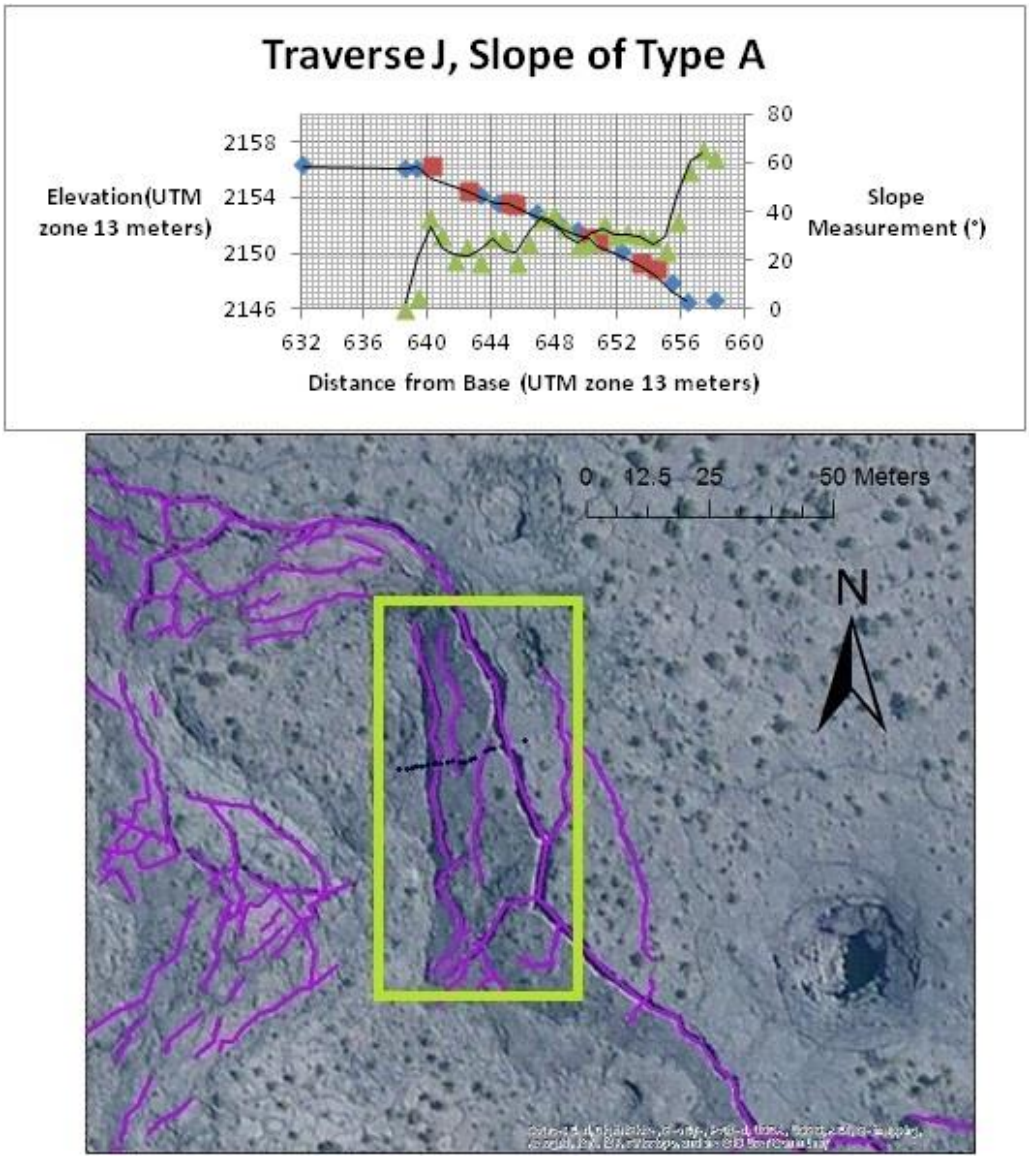

Figure 11. The graph contains the DGPS points for Traverse J, an example of a Type A crack pattern escarpment. In the graph, the blue diamonds are DGPS points and the red squares are crack markers, both relate to the left vertical axis. The green triangle represent local slope angle measurements, and relate to the right vertical axis. The black lines are moving averages of the data points they go through. The lower picture is a satellite image of the escarpment that Traverse J crossed. Type A escarpment morphology is characterized by a linear slope, linear base and one large, wide, crack near the rim, other cracks are smaller and parallel to the larger crack.

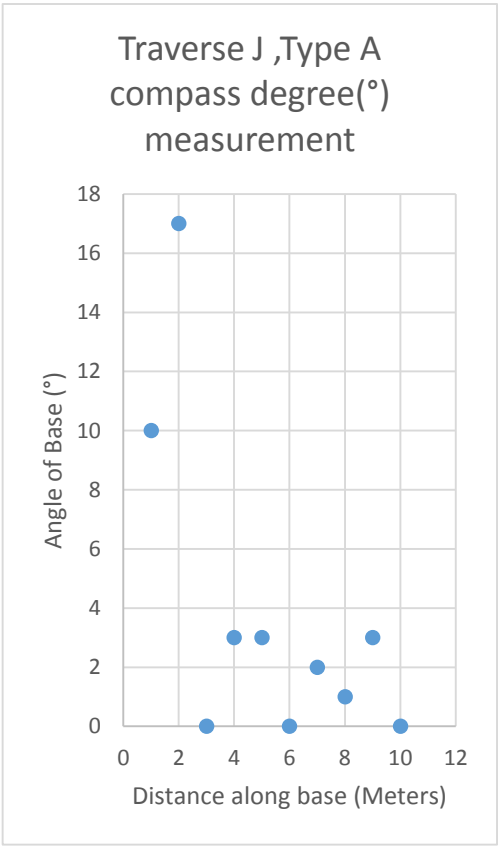

Figure 12. This graph is the base outline of Type A (Traverse J). It was created using Brunton Compass strike measurements.

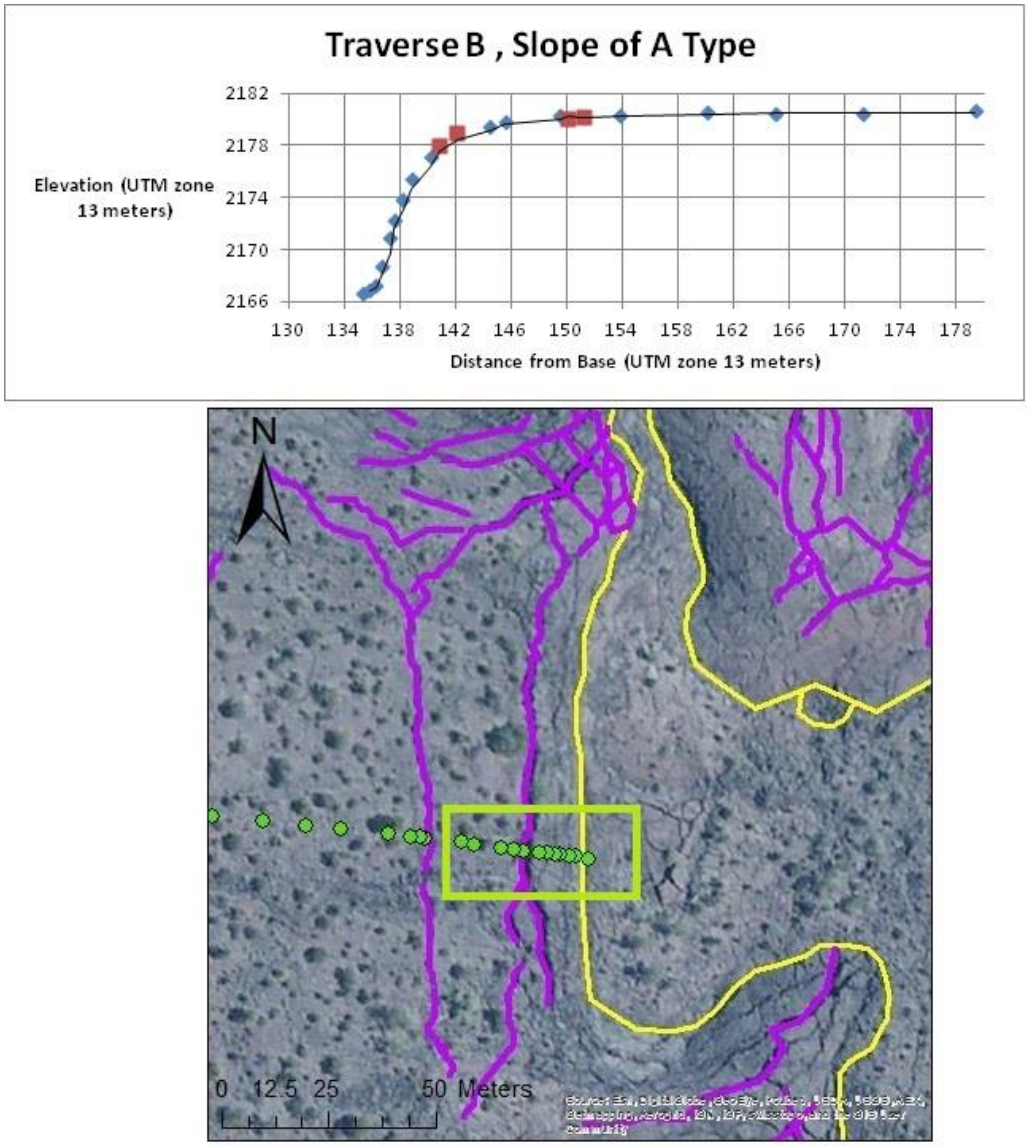

Figure 13. The graph contains the DGPS points for Traverse B, an example of a Type A crack pattern escarpment. In the graph, the blue diamonds are DGPS points and the red squares are crack markers, both relate to the left vertical axis. The black lines are moving averages of the data points they go through. The lower picture is a satellite image of the escarpment that Traverse B crossed. Type A escarpment morphology is characterized by a linear slope, linear base and one large, wide, crack near the rim, other cracks are smaller and parallel to the larger crack.

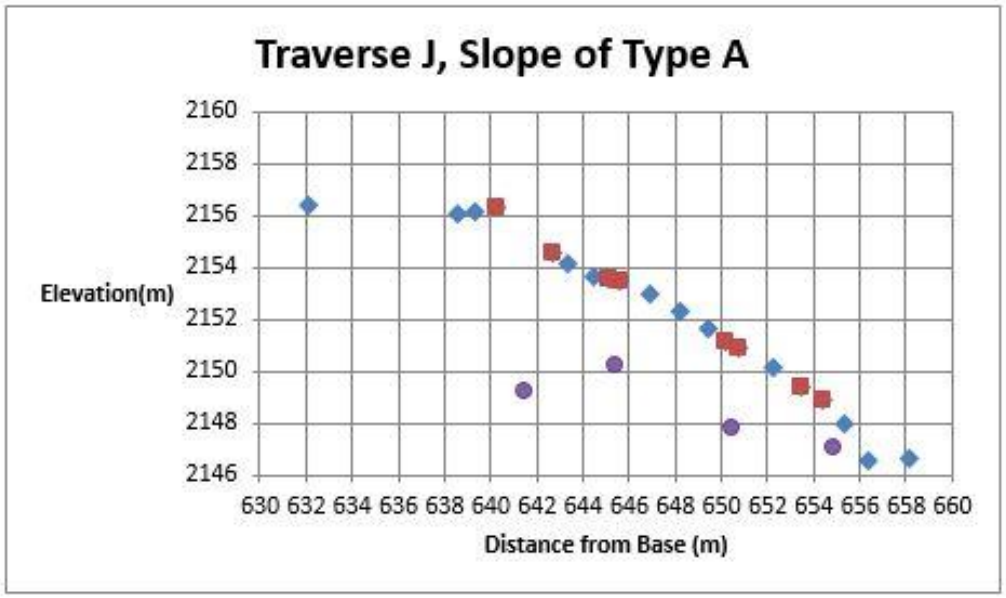

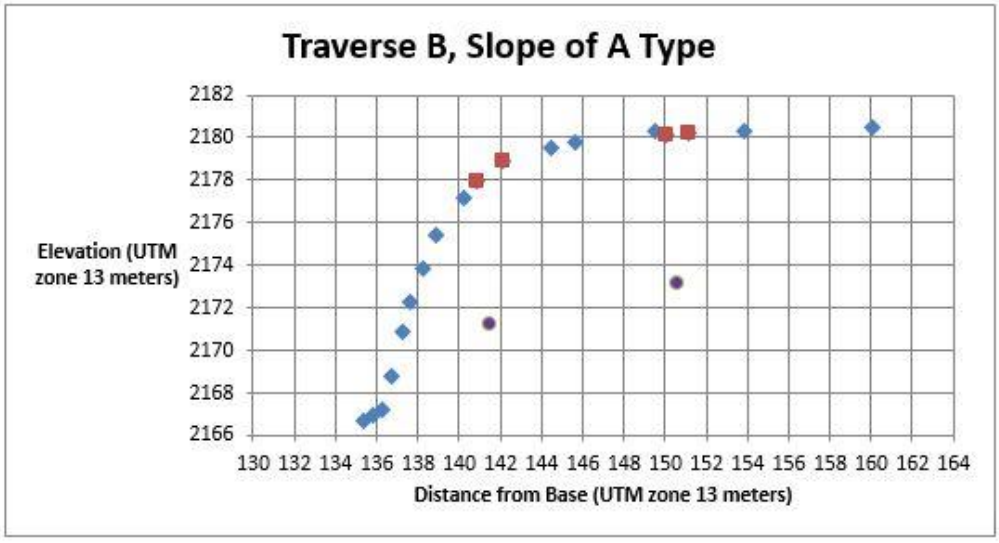

Figure 14. These two graphs show the crack depths of Type A escarpments Traverse J and Traverse B. In the graph, the blue diamonds are DGPS points, they relate to the left vertical axis. The purple circles mark the bottom of the cracks.

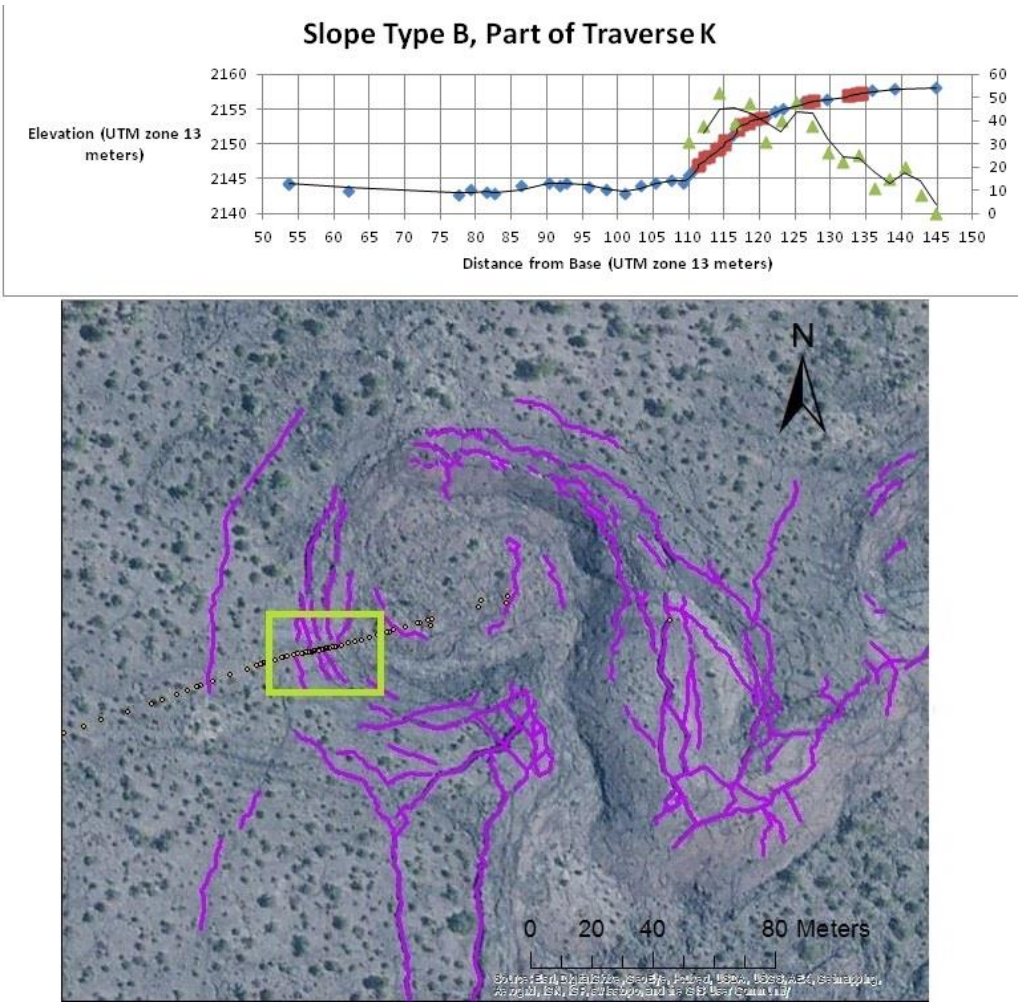

Figure 15. The graph contains the DGPS points for Traverse K, an example of a Type B crack pattern escarpment. In the graph, the blue diamonds are DGPS points and the red squares are crack markers, both relate to the left vertical axis. The green triangle represent local slope angle measurements, and relate to the right vertical axis. The black lines are moving averages of the data points they go through. The lower picture is a satellite image of the escarpment that Traverse K crossed. Type B escarpment morphology is characterized by an 'S'-shaped slope, concave base and lots of similarly sized small, thin, cracks subparallel to each other.

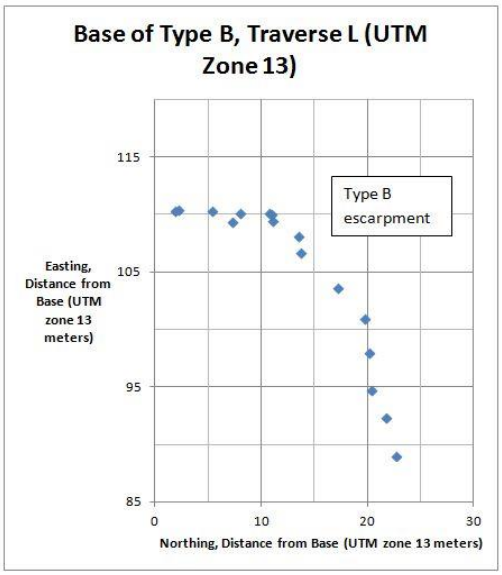

Figure 16. This graph is the base outline of Type B (Traverse L). It was created using DGPS points.

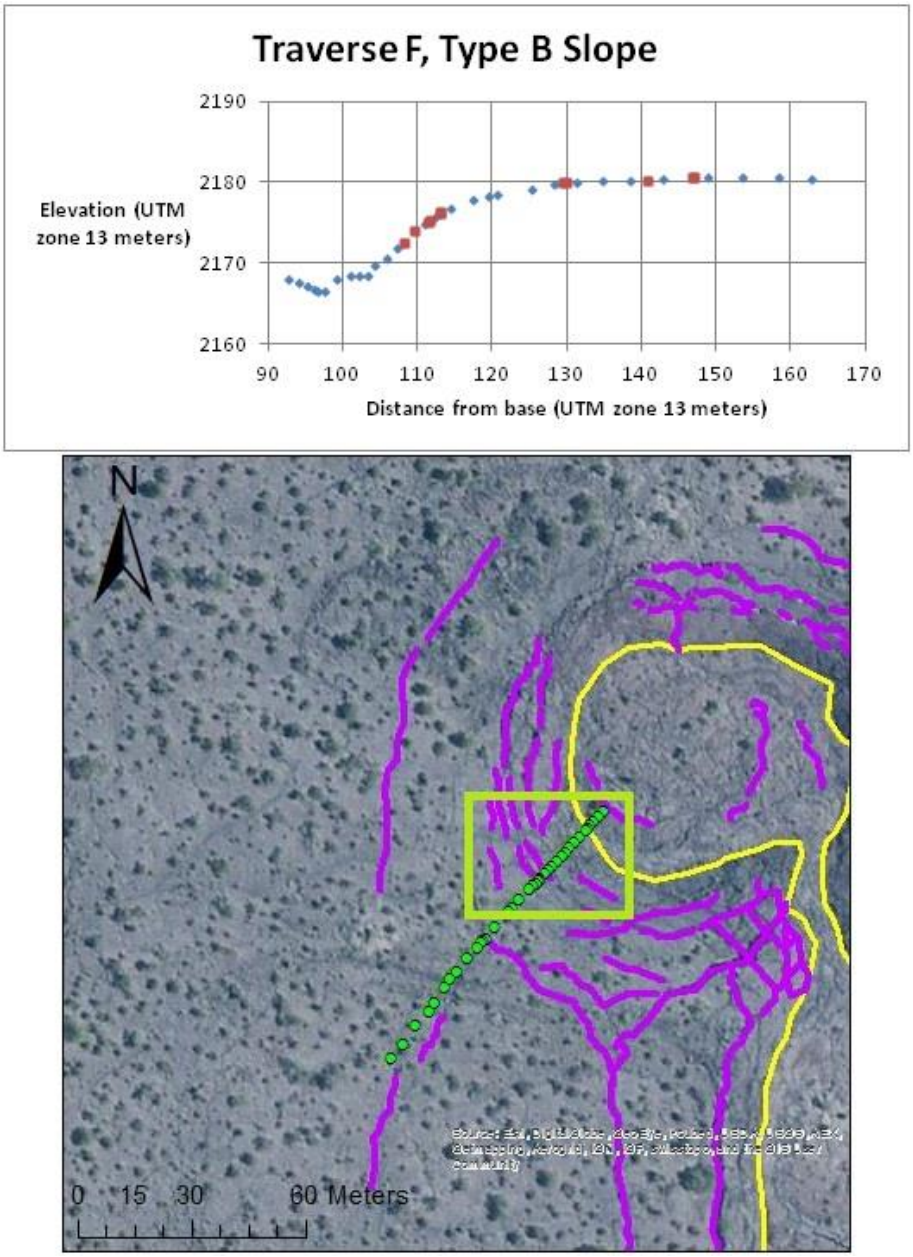

Figure 17. The graph contains the DGPS points for Traverse F, an example of a Type B crack pattern escarpment. In the graph, the blue diamonds are DGPS points and the red squares are crack markers, both relate to the left vertical axis. The black lines are moving averages of the data points they go through. The lower picture is a satellite image of the escarpment that Traverse F crossed. Type B escarpment morphology is characterized by an 'S'-shaped slope, concave base and lots of similarly sized small, thin, cracks subparallel to each other.

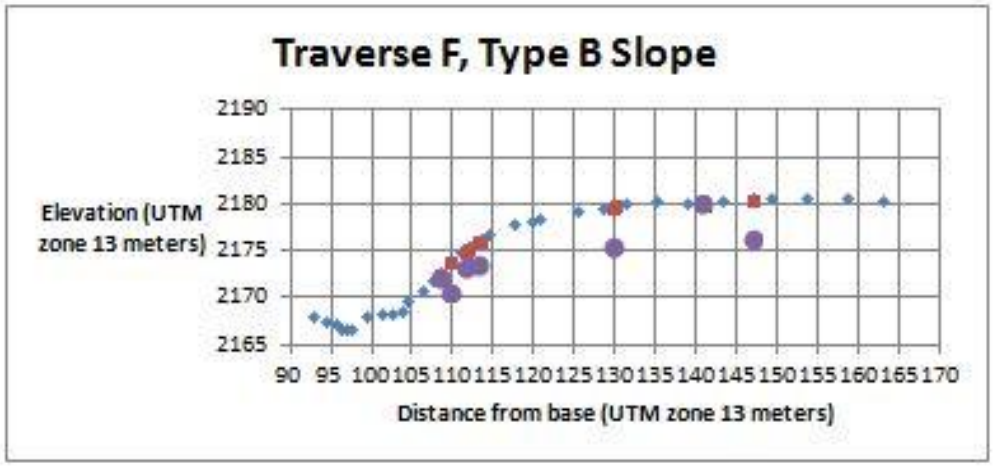

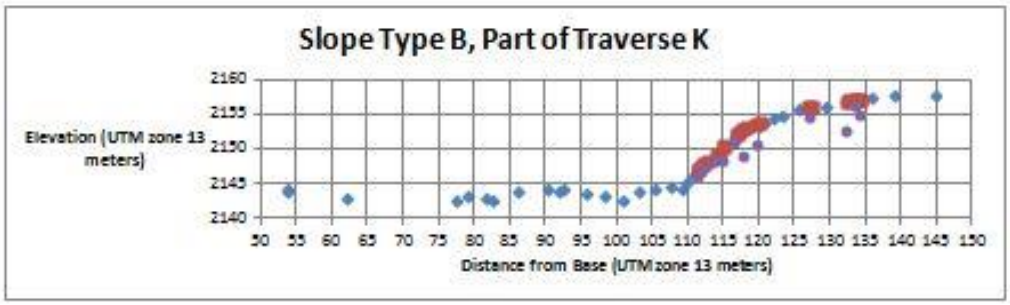

Figure 18. These two graphs show the crack depths of Type B escarpments Traverse F and Traverse K. In the graph, the blue diamonds are DGPS points, they relate to the left vertical axis. The purple circles mark the bottom of the cracks.

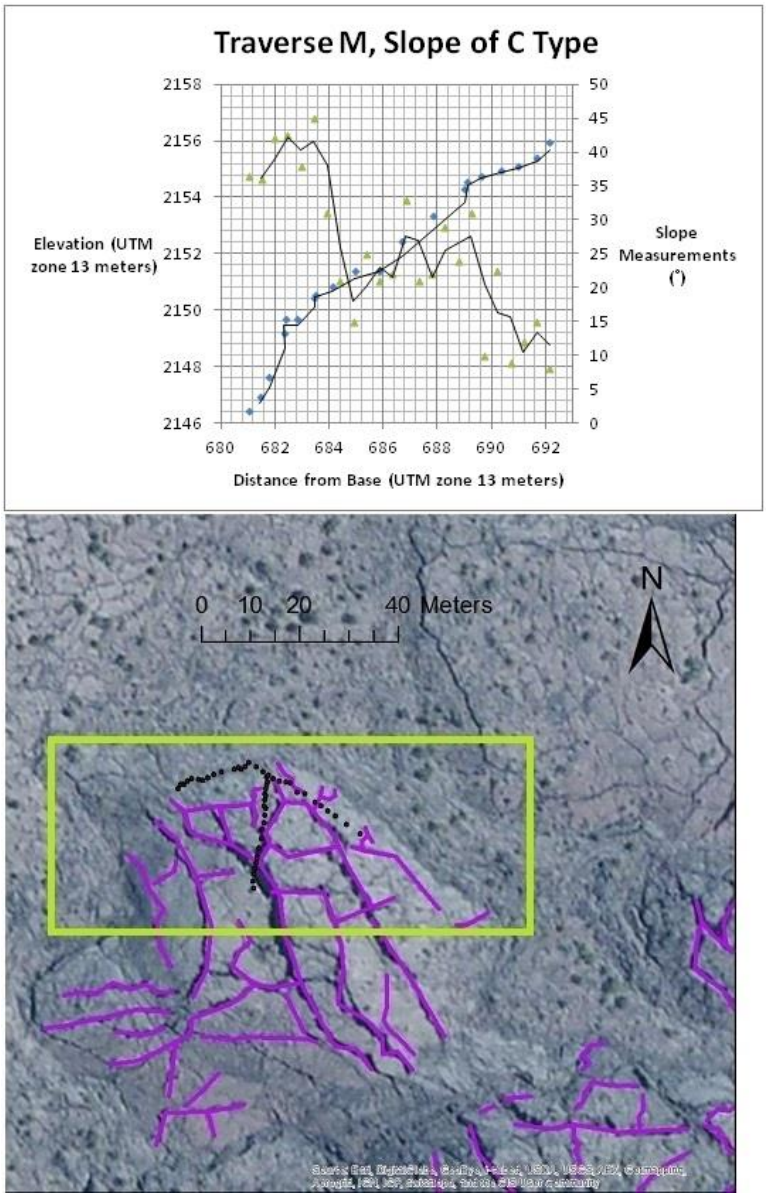

Figure 19. The graph contains the DGPS points for Traverse M, an example of a Type C crack pattern escarpment. In the graph, the blue diamonds are DGPS points, they relate to the left vertical axis. The green triangle represent local slope angle measurements, and relate to the right vertical axis. The black lines are moving averages of the data points they go through. No cracks are marked in the graph for this slope because traverses are not accurate measurement the polygonal crack pattern seen on Type C escarpments. The lower picture is a satellite image of the escarpment that Traverse M crossed. Type C escarpment morphology is characterized by a convex slope, convex base and many polygonal, intersecting cracks of various widths.

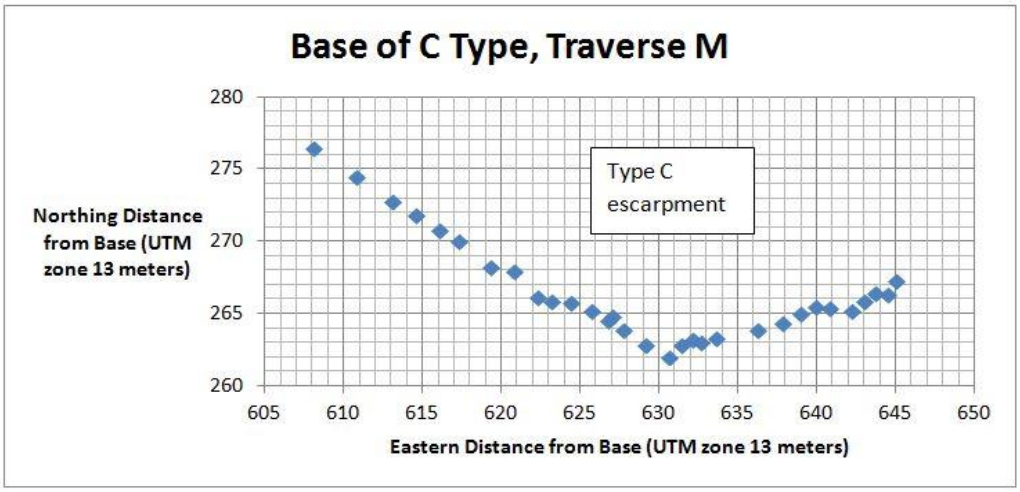

Figure 20. This graph is the base outline of Type C (Traverse M). It was created using DGPS points.

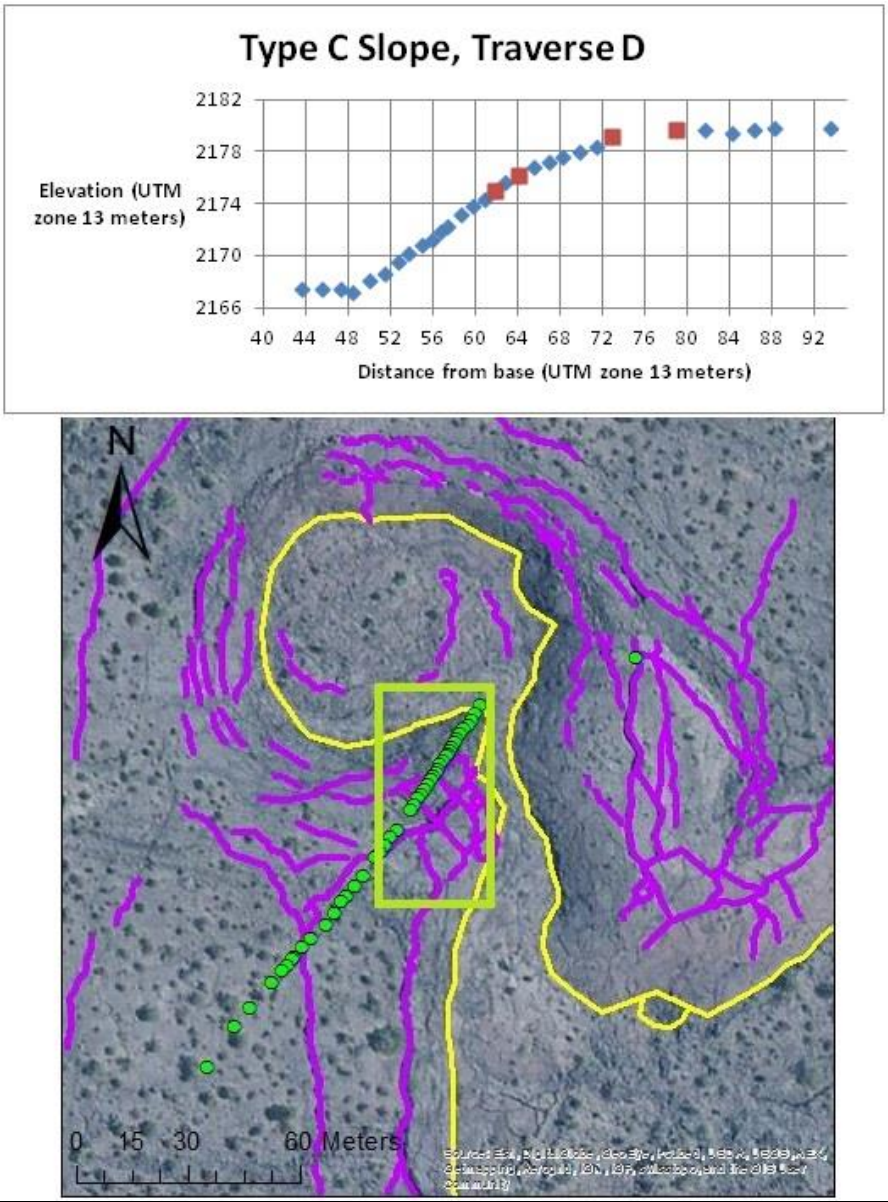

Figure 21. The graph contains the DGPS points for Traverse D, an example of a Type C crack pattern escarpment. In the graph, the blue diamonds are DGPS points, they relate to the left vertical axis. The black lines are moving averages of the data points they go through. No cracks are marked in the graph for this slope because traverses are not accurate measurement the polygonal crack pattern seen on Type C escarpments. The lower picture is a satellite image of the escarpment that Traverse D crossed. Type C escarpment morphology is characterized by a convex slope, convex base and many polygonal, intersecting cracks of various widths.

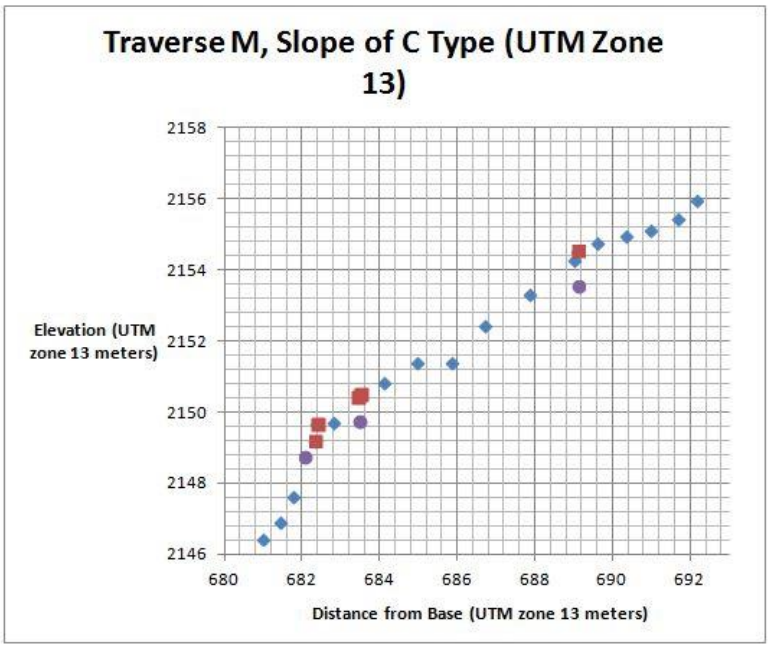

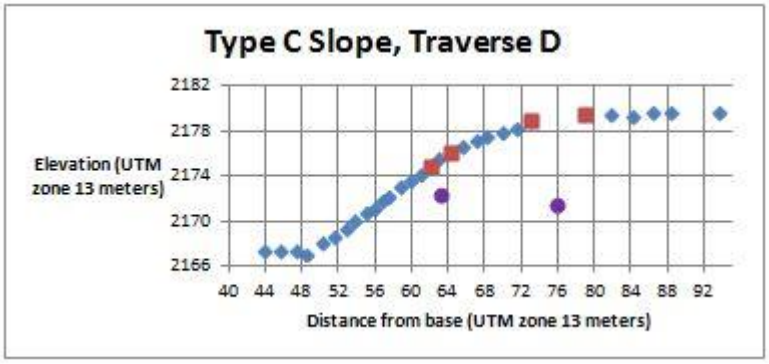

Figure 22. These two graphs show the crack depths of Type C escarpments Traverse M and Traverse D. In the graph, the blue diamonds are DGPS points, they relate to the left vertical axis. The purple circles mark the bottom of the cracks.

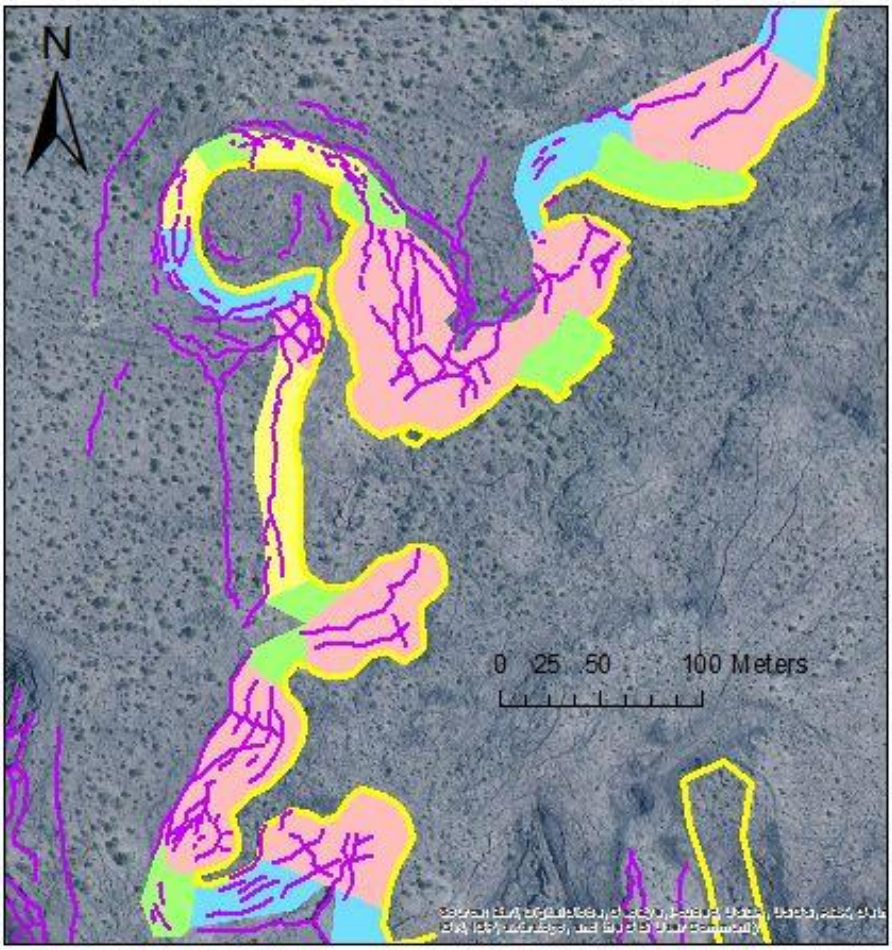

Figure 23. An image of part of the mapped and identified crack type slopes on the eastern side of the McCartys flow. Magenta lines are cracks visible in the satellite imagery; yellow lines indicate margin outlines. Yellow indicates an escarpment section of crack Type A; blue indicates an escarpment section of crack Type B; pink indicates an escarpment section of crack Type C; green indicates questionable/non-crack type section. Only the escarpments of the inflation plateau are mapped. The yellow lines mark the edges of the margins, the bottom of the escarpments.

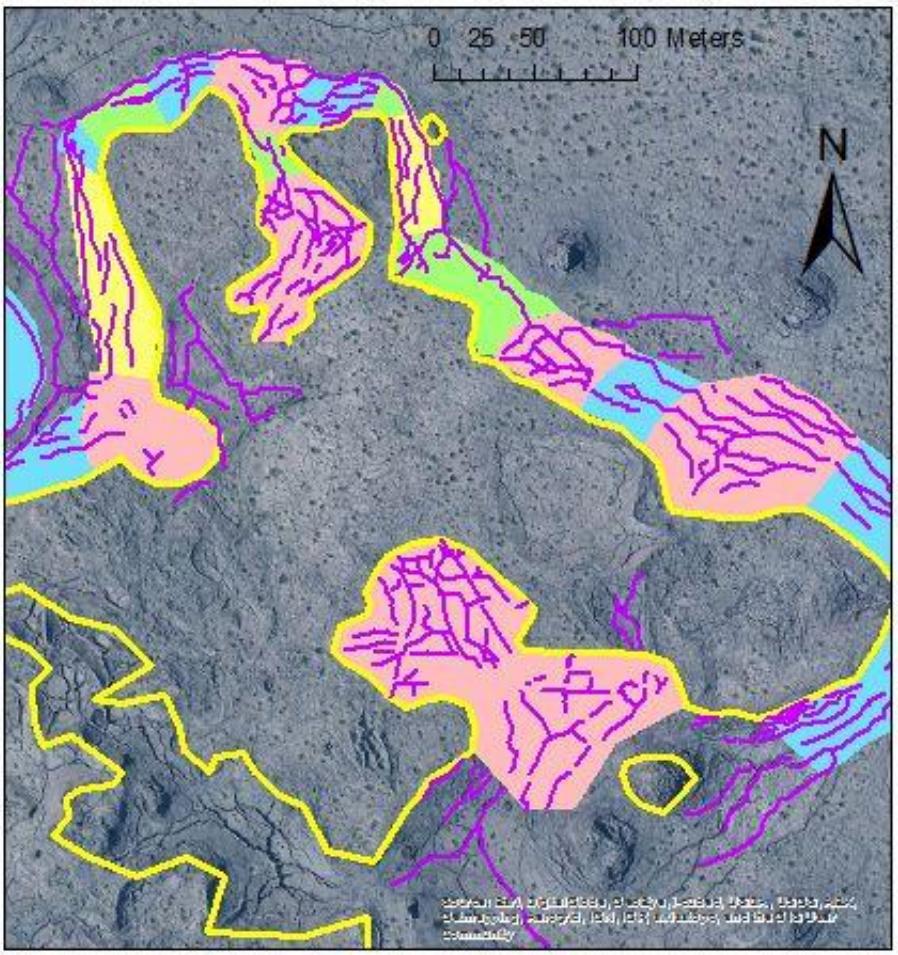

Figure 24. An image of part of the mapped and identified crack type slopes on the western side of the McCartys flow. Magenta lines are cracks visible in the satellite imagery; yellow lines indicate margin outlines. Yellow indicates an escarpment section of crack Type A; blue indicates an escarpment section of crack Type B; pink indicates an escarpment section of crack Type C; green indicates questionable/non-crack type section. Only the escarpments of the inflation plateau are mapped. The yellow lines mark the edges of the margins, the bottom of the escarpments. The yellow outlined inflated unit in the bottom left corner of the image is best called a pressure ridge, it is not an escarpment to the inflation plateau and is therefore not included in the survey.

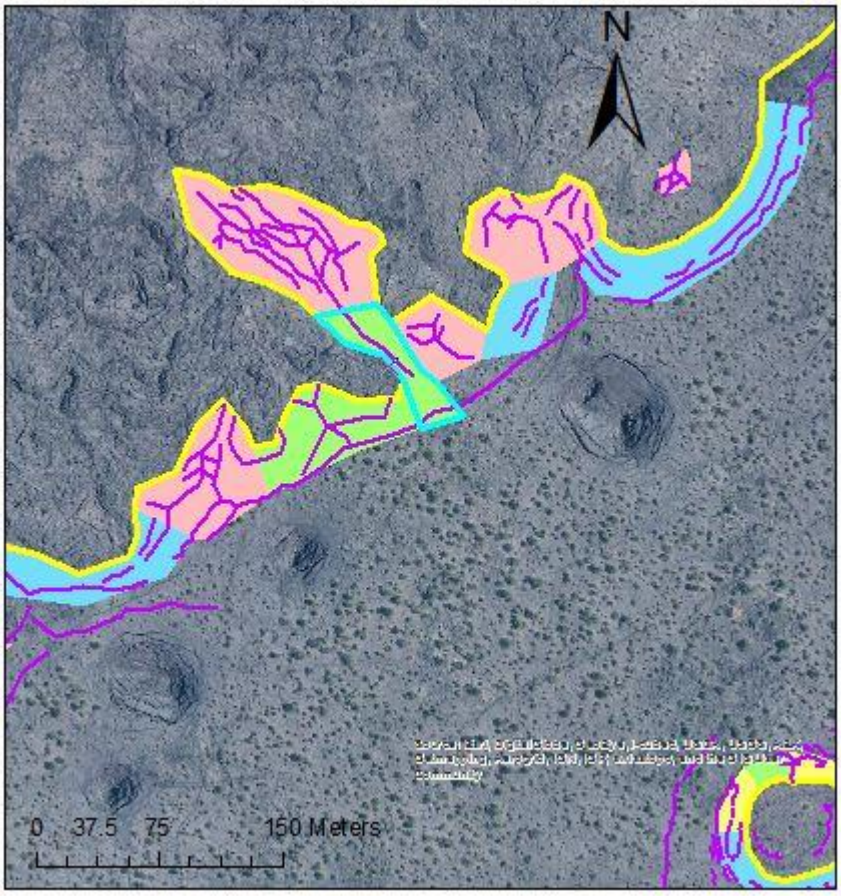

Figure 25. An image of part of the mapped and identified crack type slopes slightly to the north of original field sight, seen in the bottom right of the image. Magenta lines are cracks visible in the satellite imagery; yellow lines indicate margin outlines. Yellow indicates an escarpment section of crack Type A; blue indicates an escarpment section of crack Type B; pink indicates an escarpment section of crack Type C; green indicates questionable/non-crack type section. Only the escarpments of the inflation plateau are mapped. The yellow lines mark the edges of the margins, the bottom of the escarpments.

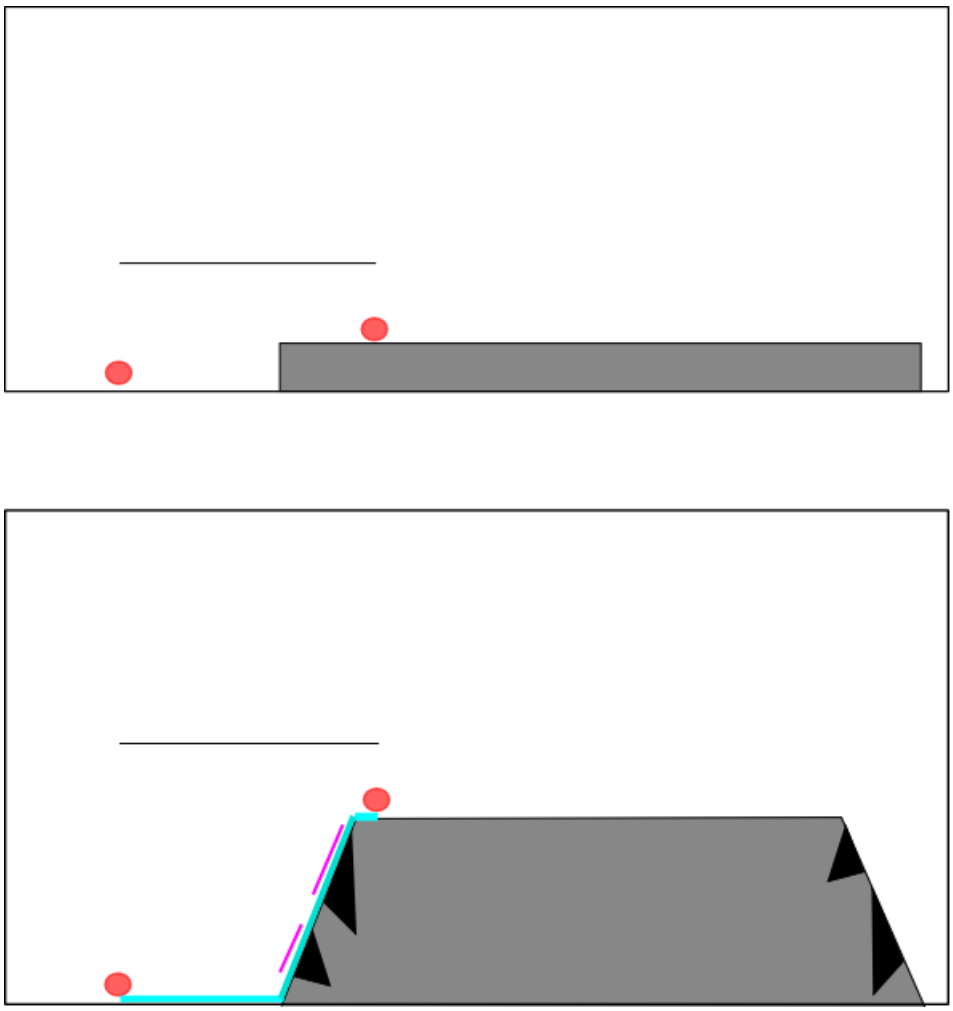

Figure 26. The upper image shows a sheet flow pre-inflation. The red dots mark two spots, one on the sheet flow that inflates and one on a section that will not inflate) with a constant distance between them (the black horizontal line). The grey trapezoid is the inflated plateau, the black triangles are two cracks, the magenta lines are the width of the cracks and the blue line is the surface connection between the two spots. The idea behind this sketch is that in the idealized model of an inflation plateau where spots on top of the plateau are merely vertically uplifted. Therefore if the cracks were collapsed and the plateau deflated the spot on the plateau and off the plateau are still the same distance apart. The width of the cracks on an inflation plateau should be equal to the uplift of the plateau.

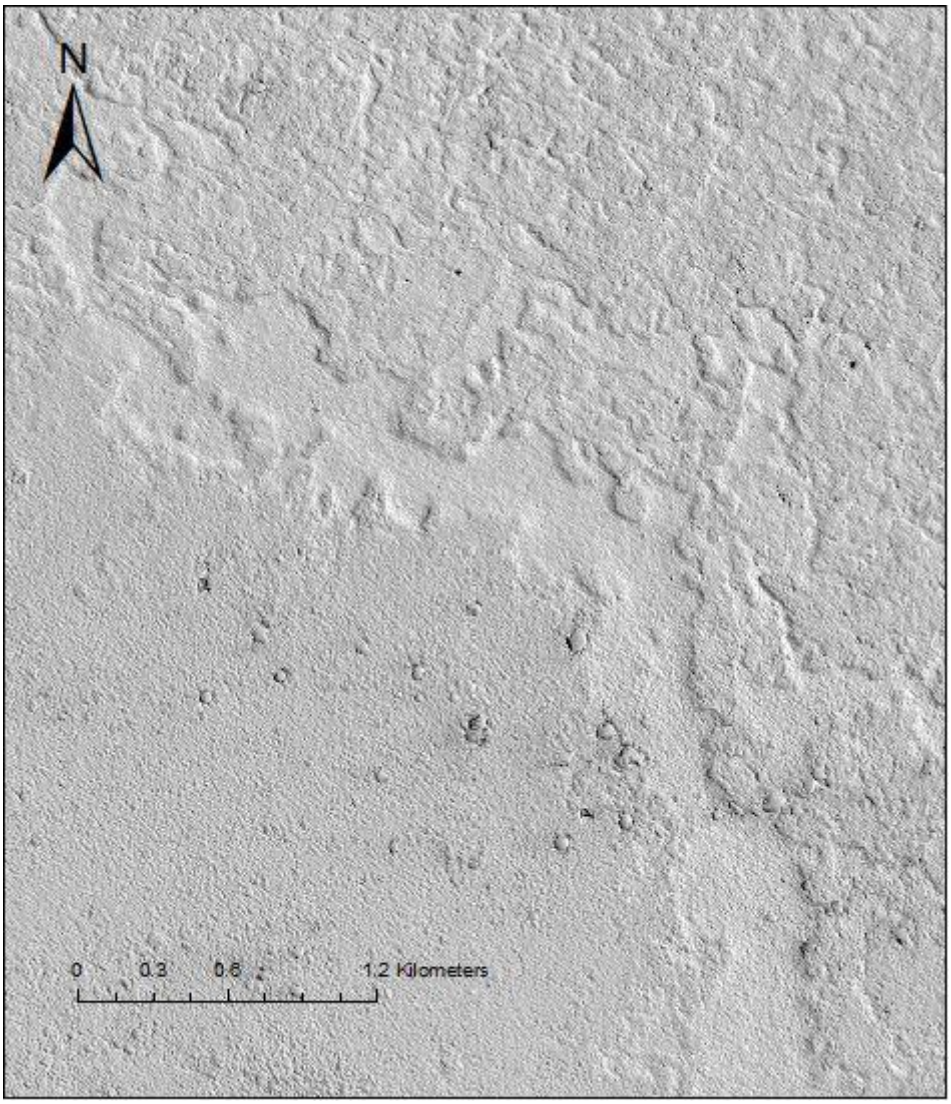

Figure 27. This inflation plateau was identified by Keszthelyi et al., 2008. The bottom left of the image is uninflated terrain, the top right has inflated sections. NASA/JPL/University of Arizona.

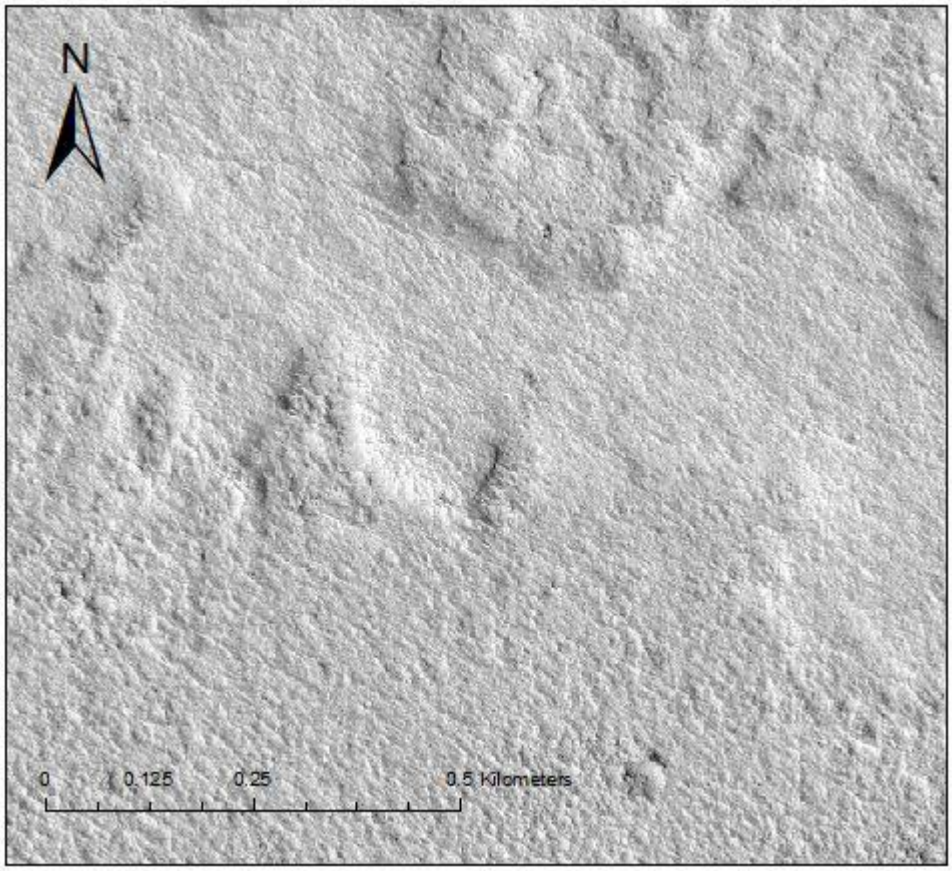

Figure 28. This image is the red box in Figure 43; it is a zoomed in view of the inflation plateau identified by Keszthelyi et al., 2008. NASA/JPL/University of Arizona.

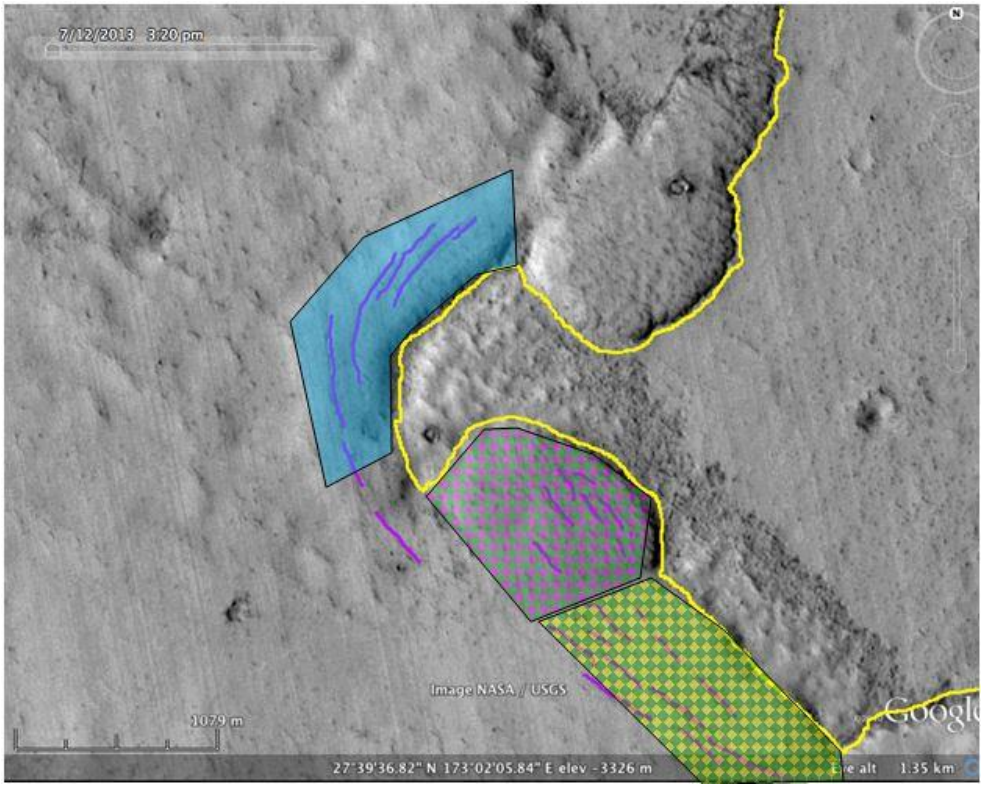

Figure 29. This figure is an image of crack on the surface of Mars 200km north-east of the Phlegra Dorsa area near Elysium. Magenta lines denote the cracks; the yellow line denotes what I believe to be the margin of the inflated feature. The blue shape is the outline of a section I believe to have a Type B crack pattern, the pink and green checkered shape marks what I tentatively believe to be a Type C crack pattern, and the yellow and green checkered shape marks what I tentatively believe to be a Type A crack pattern section. Cracks are much harder to discern in this image from GoogleMars than images of Earth. The tentative Type C section is the most difficult in this image because it is a little too blurry to differentiate between surface textures and cracks. Note the scale in the bottom left is 1079m.

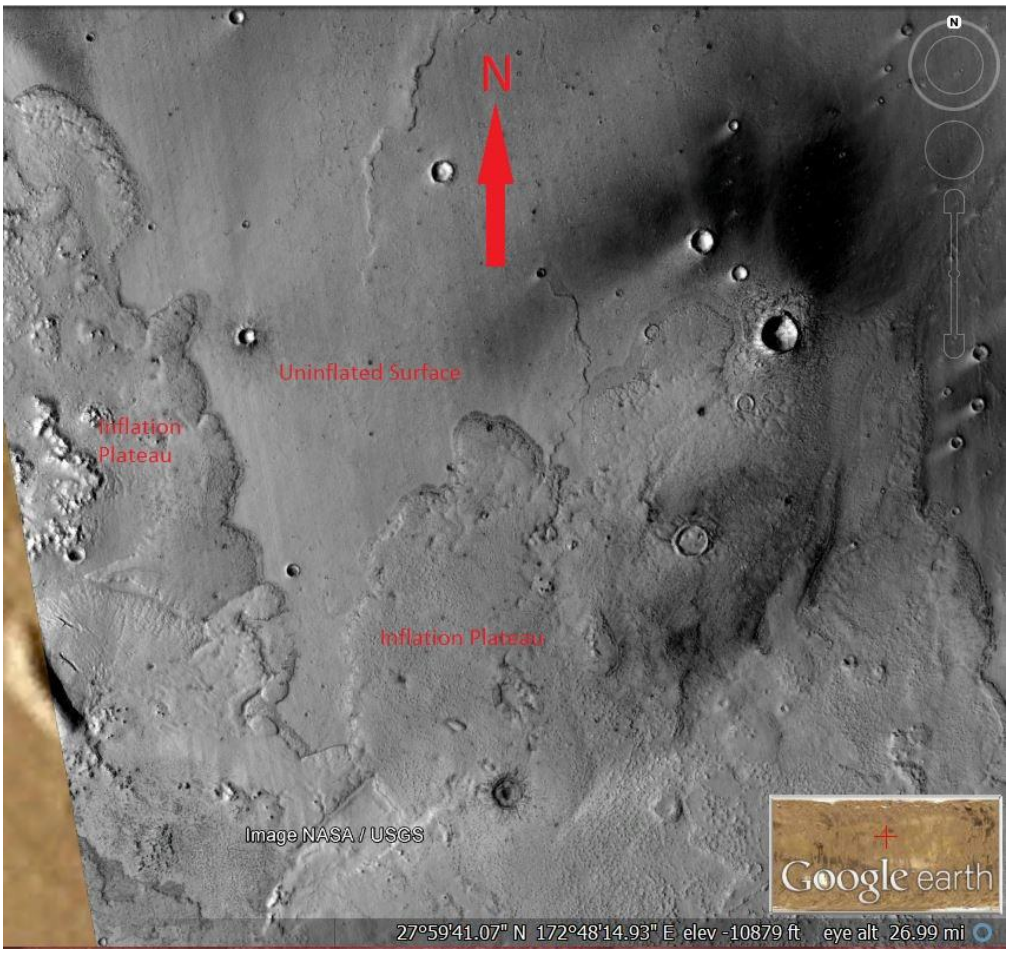

Figure 30. This image from Google Mars is of an inflation plateau identified by Andy deWet (Personal Communication, Andy deWet, 2014). Figure 29 is an image of the area in the red box.

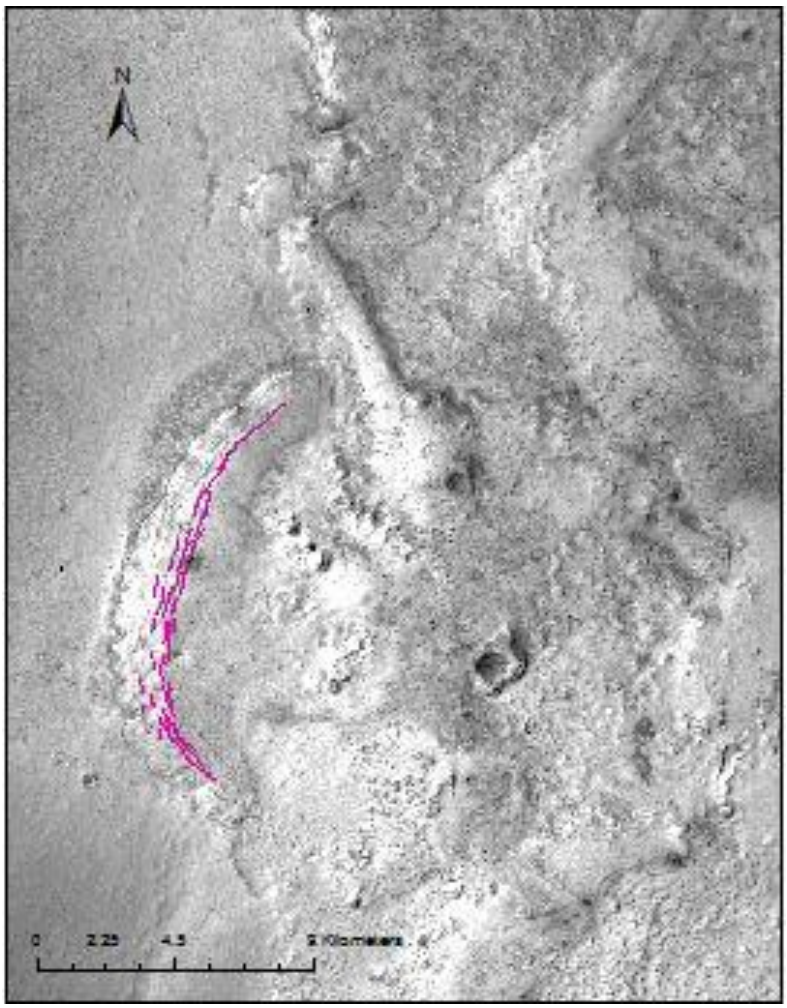

Figure 31. The feature on the left of the images is most likely an inflation ridge. The magenta lines highlight cracks on the feature. The scale on the bottom left is 2 kilometers. Andy deWet Personal Communication, 2014. NASA/JPL/University of Arizona.

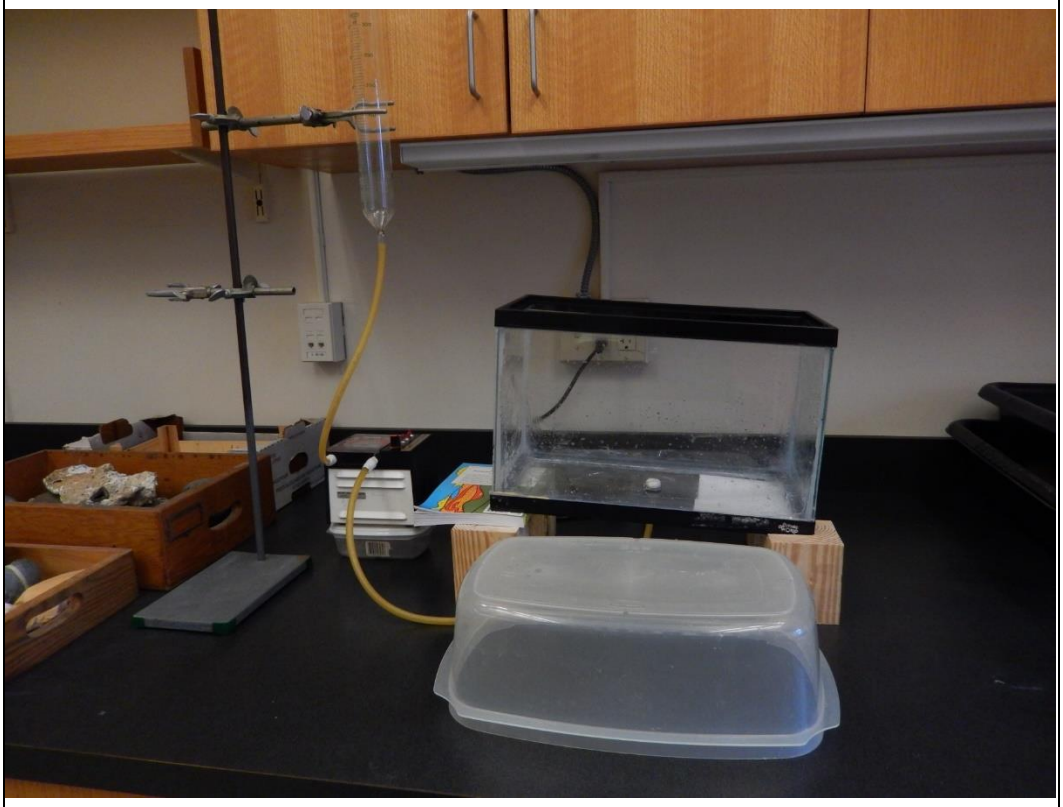

Figure 32. Analog model set up. The suspended vial held the blue dyed liquid wax. There was a putty plug over the vent. The thin book under the side of the tank on the left of the photo that provided the 1.98°. The upside down tub was used as a rest for the video camera.

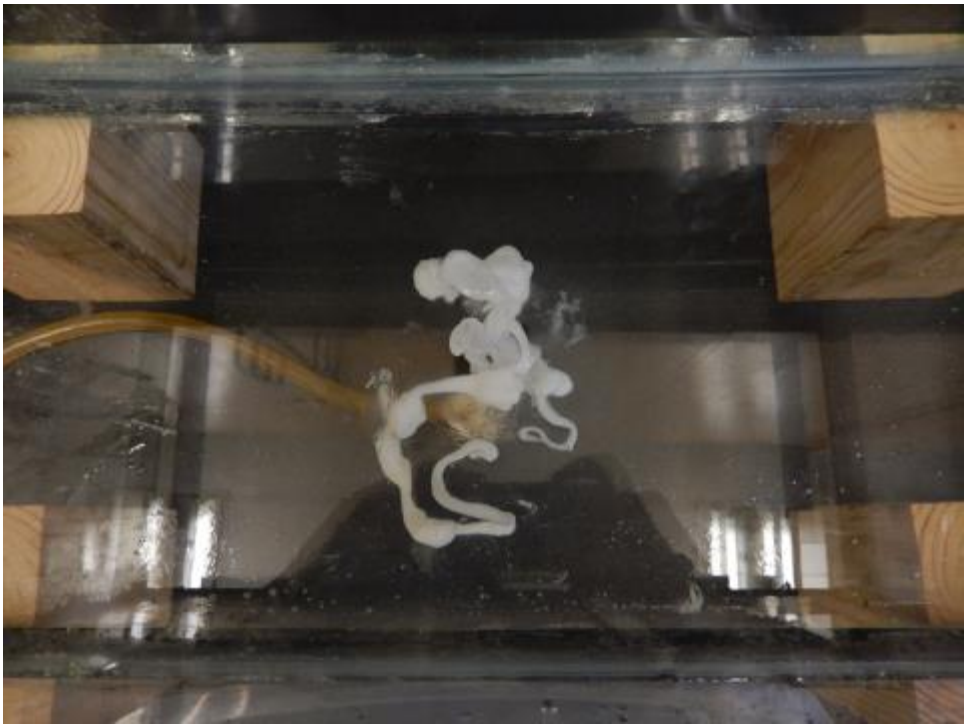

Figure 33. Trial 1 of PEG wax analog initial output. The tubes of wax floated in the sucrose solution with a density of 113.3/g/ml.

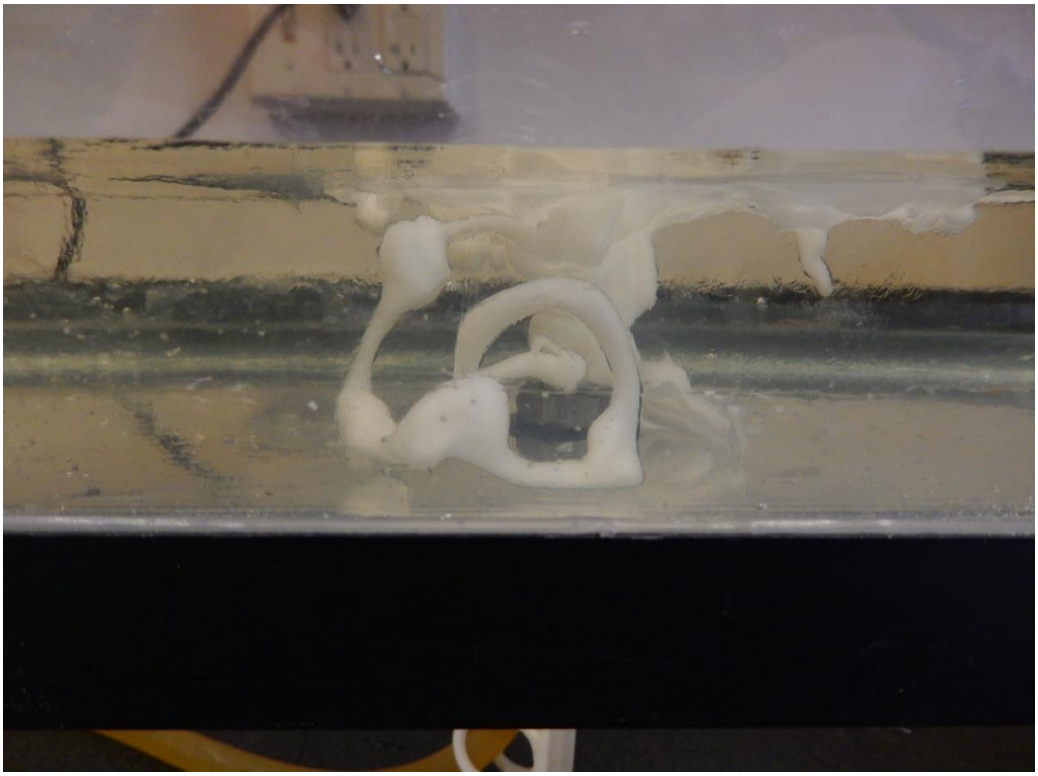

Figure 34. Trial 1 of PEG wax analog model. Side view of figure 33.

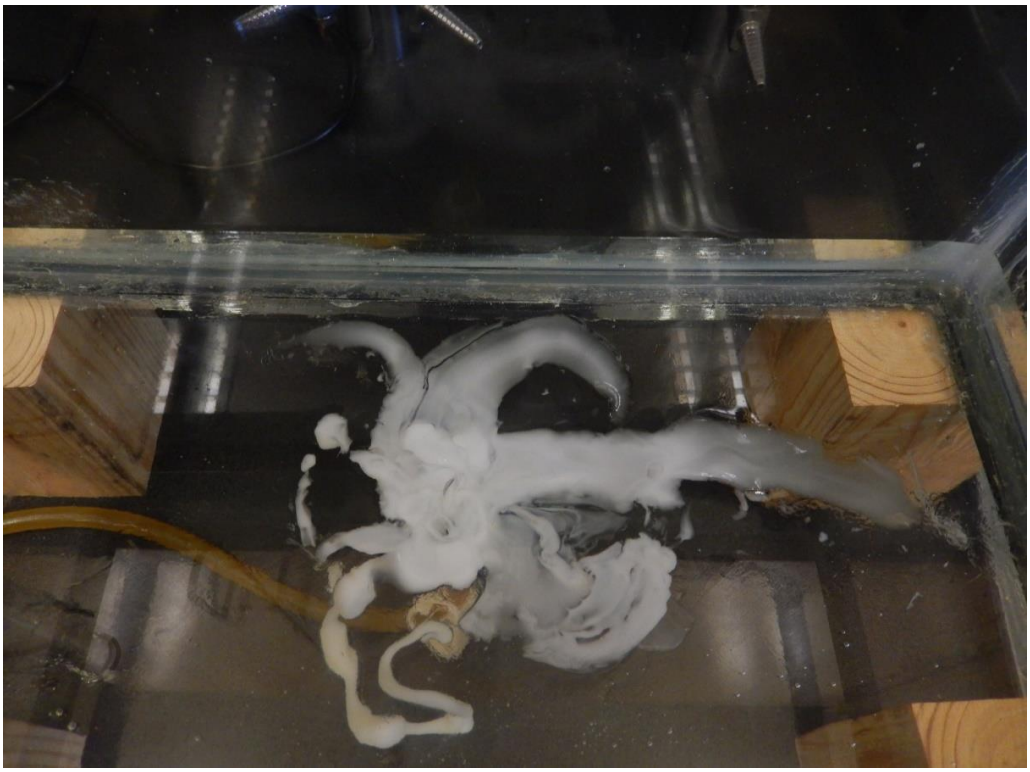

Figure 35. Trial 1 PEG wax analog. Final appearance of PEG wax. There is a large clump above the vent and thin layers floating across the top of the sucrose solution.

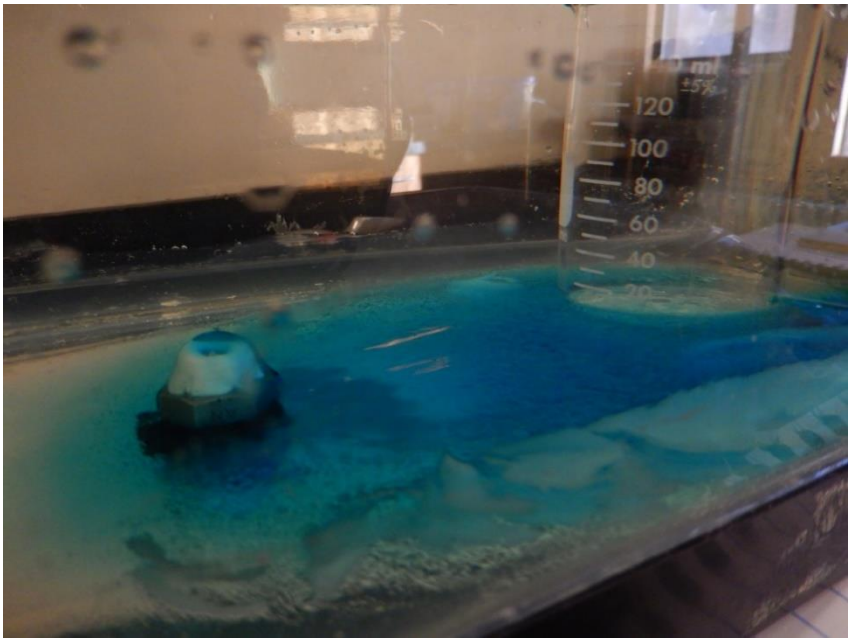

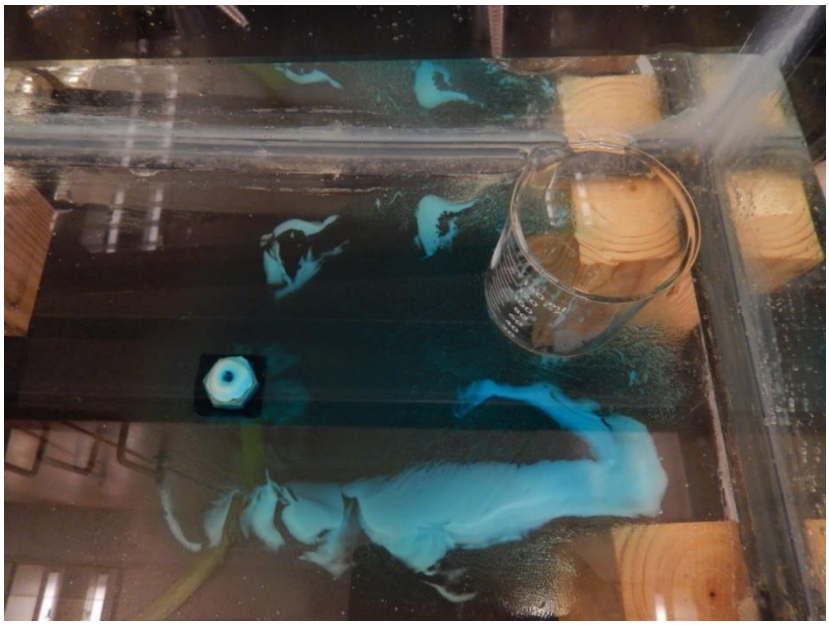

Figure 36. Trial 3 PEG wax analog model. The 150ml Pyrex beaker was placed in the liquid wax part of the flow and filled with sucrose solution so it stunk to the bottom of the tank. The solid wax sections in these images formed with the initial flow. The middle part of the flow remained liquid and never solidified.

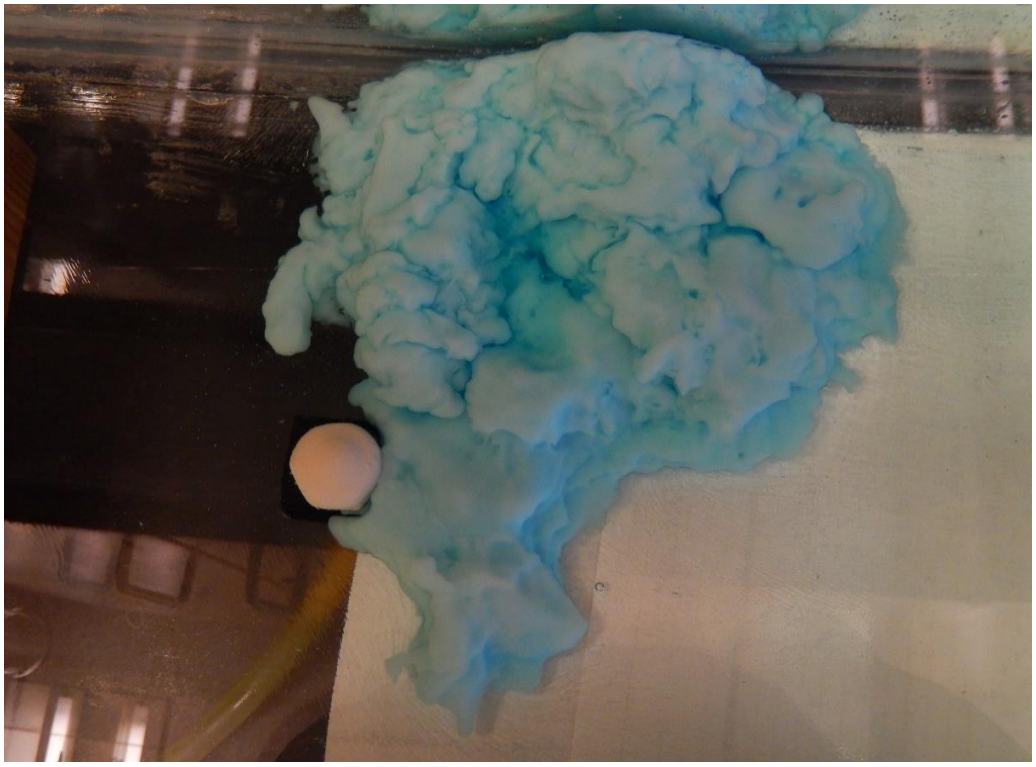

Figure 37. Trial 4 PEG wax analog model. This image was taken after the flow lobes hit the wall of the tank and then proceeded to flow uphill. The wax inside the black circle is a liquid wax sitting on top of the flow. This pool of liquid wax never solidified because the temperature of the sucrose solution had become too warm to allow the wax to solidify.

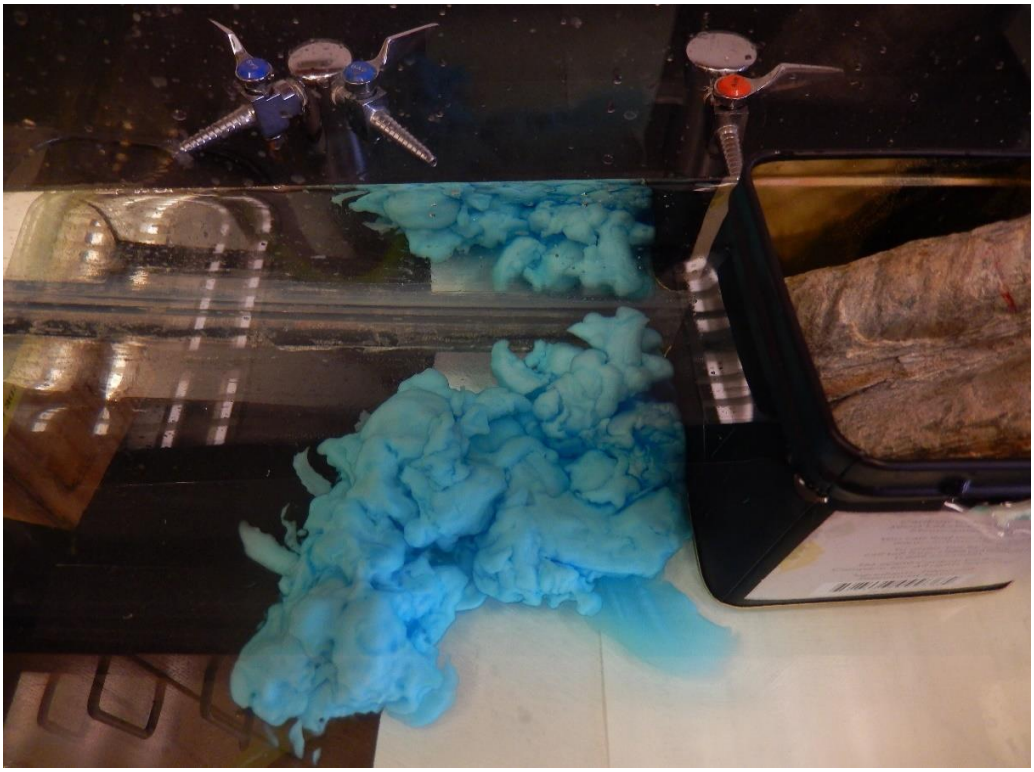

Figure 38. Trial 5 PEG wax analog model. The vent, located in the lower left of the picture, is completely coved in wax. The square tin, has a rock inside it to way it down. The solidified wax in the top of the picture is flowing up against the square tin. Towards the bottom of the photo, a thin, 1-2m tall, lobe of wax flowed out from under the wax flow.

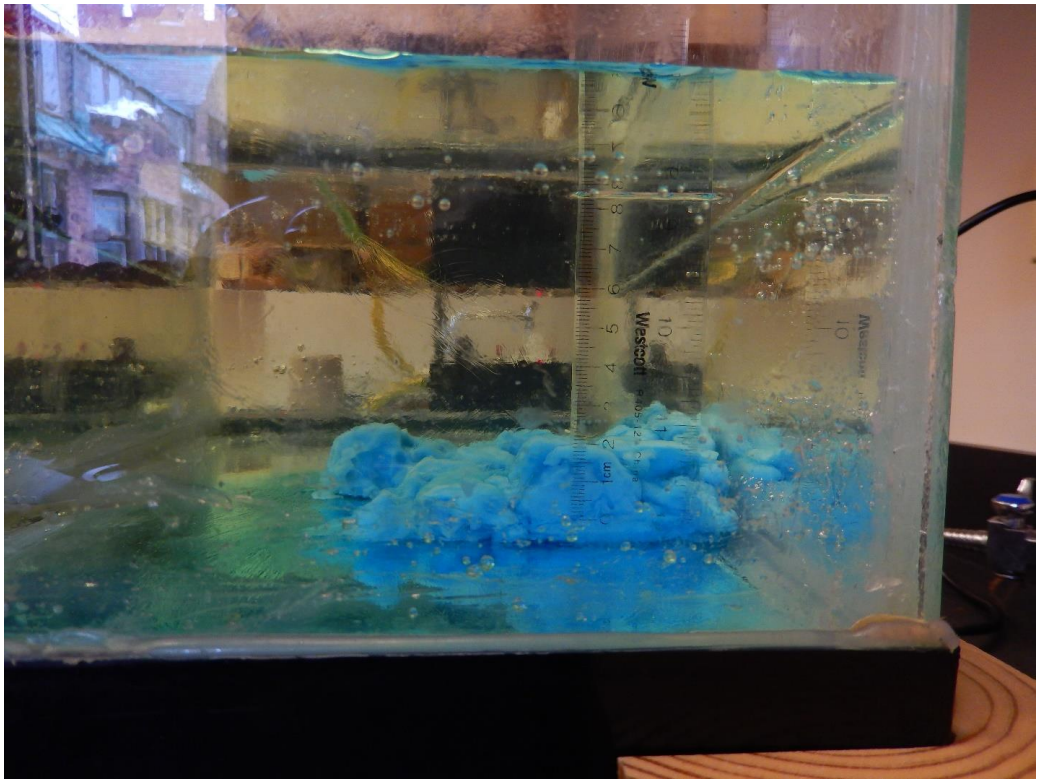

Figure 39. Trial 5 PEG wax analog model. This is an end view of the flow after the square tin was removed. The ruler shows the flow piled up to 2cm next to the square tin.

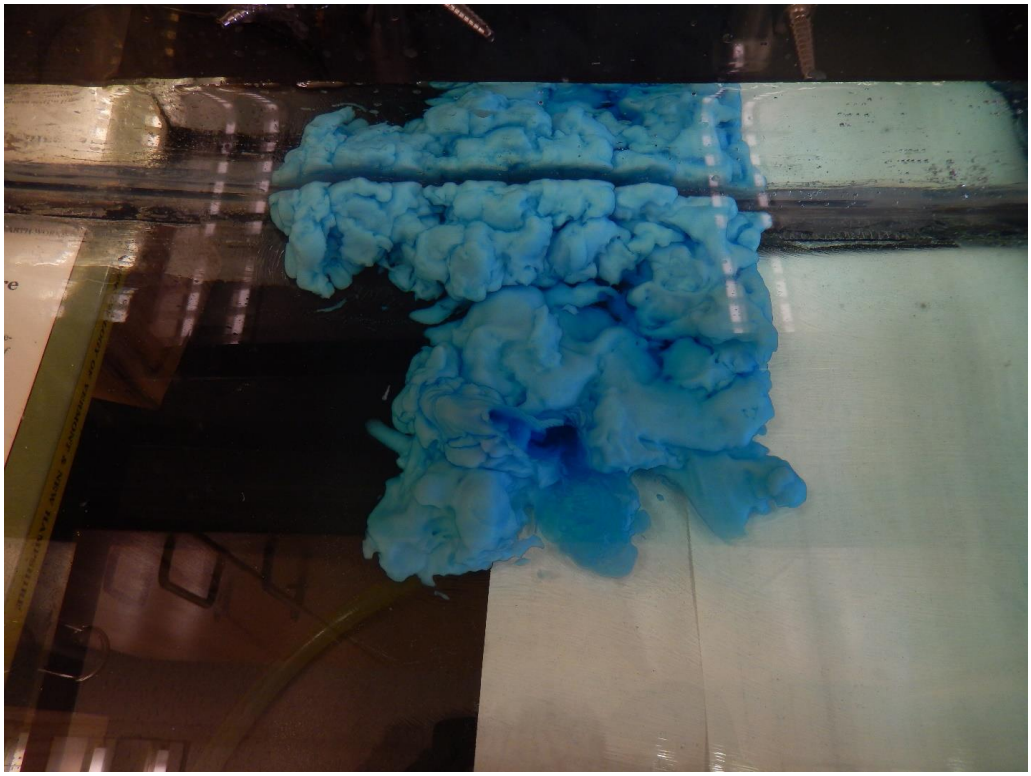

Figure 40. Trial 5 PEG wax analog model. This photo was taken after the square tin was removed. The wax up against the tank near the top of the photo flowed uphill. The new breakout of liquid wax is near the vent. It is still clear in this photo and therefore the crust is not fully solidified like the crust of the rest of the flow.

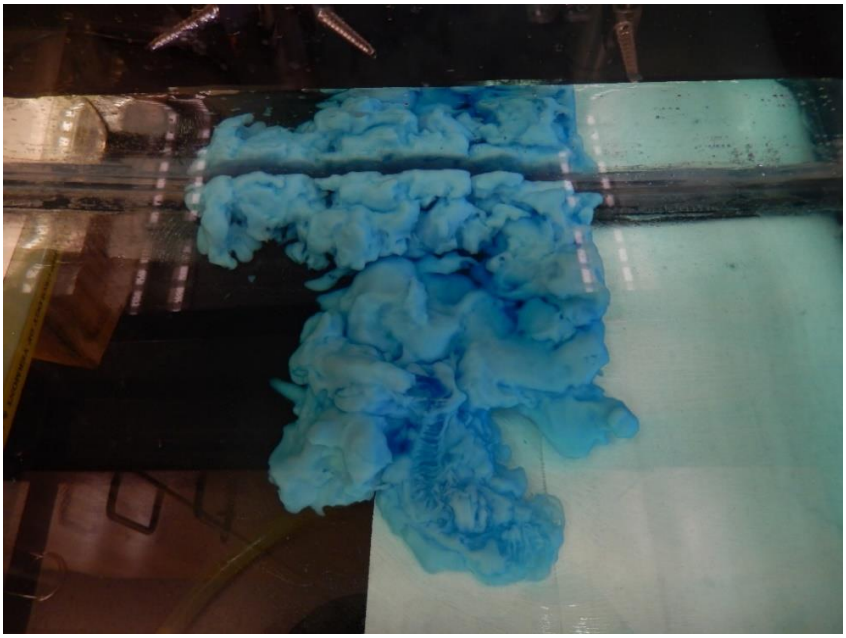

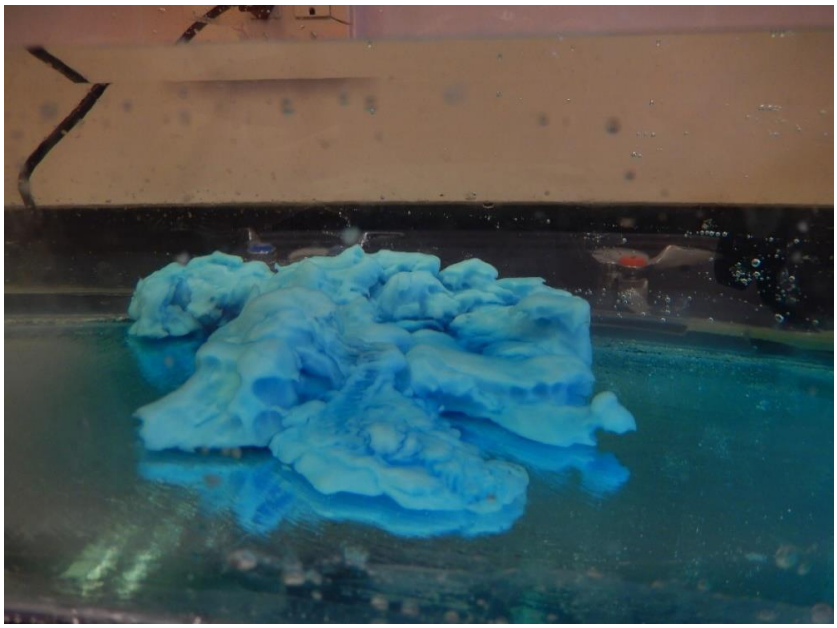

Figure 41. Trial 5 PEG wax analog model. These photos show the final stage of the analog model. The wax has rounded and eroded slightly over the course of the trial run. The last lobe has a center channel with the appearance of a staircase.

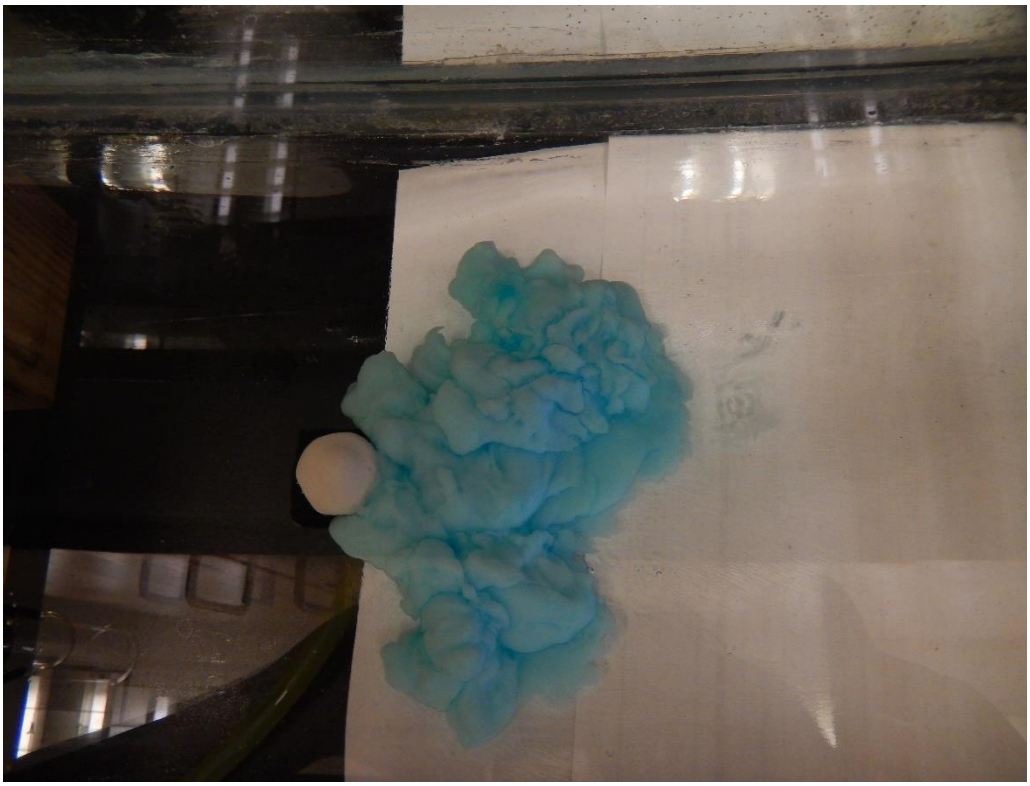

Figure 42. Trial 4 PEG wax analog model. The lobes of wax all have solidified upper crusts and have spread downhill and laterally.

REFERENCES

Applegarth, L. J., James, M.R., van Wyk de Vries, B., and H. Pinkerton. (2009) Influence of surface clinker on the crustal structures and dynamic of ’a’ā lava flows. *Journal of Geophysical Research* 115.

Balmforth, N.J., Burbidge, A.S., Craster, R.V., Salzig, J. and A. Shen. (2000) Visco-plastic models of isothermal lava domes, Journal Fluid Mechanics: 403: 37-65.

Blake, S. and Bruno, B.C. (2000) Modelling the emplacement of compound lava flows. *Earth and Science Letters* 184: 181-197.

Carden, J.R. and Laughlin, A.W. (1974). Petrochemical variations within the McCartys lava flow, Valencia County, New Mexico. *Geological Society of America Bulletin*. 85: 1479-84.

Champion, D.E., and Greeley, R. (1977) Geology of the Wapi lava field, Snake River Plain, Idaho, in Greeley, R., and King, J. S., eds., Volcanism of the eastern Snake River Plain, Idaho: A comparative planetary geology guidebook: Washington, D.C., National Aeronautics and Space Administration, p.133-152.

Crown, D.A. and Baloga, S.M. (1999) Pahoehoe toe dimensions, morphology, and branching relationships at Mauna Ulu, Kilauea Volcano, Hawai’i. *Bull Volcanol* 61: 288-305.

Dunbar, Nelia W. and Fred M. Phillips (2004) Cosmogenic ^{36}Cl ages of lava flows in the Zuni-Bandera volcanic field, north-central New Mexico, U.S.A, New Mexico Bureau of Geology & Mineral Resources, Bulletin 160.

Fink, Jonathan H., and Griffiths, Ross W. (1990) Radial spreading of viscous-gravity currents with solidifying crust. *Journal of Fluid Mechanics* 221:485-509.

Garry, Brent W., Zimbelman, James R. and Tracey K. P. Gregg (2007) Morphology and emplacement of a long channeled lava flow near Ascraeus Mons Volcano, Mars. *Journal of Geophysical Research* 112.

Glaze, Lori S., and Baloga, Stephen M. (2013) Simulation of Inflated Pahoehoe Lava Flows." *Journal of Volcanology and Geothermal Research* 255.0:108-23.

Gregg, Tracey K.P. and Fink, Jonathan H. (2000) A laboratory investigation into the effects of slope on lava flow morphology. *Journal of Volcanology and Geothermal Research* 96:145-159.

Ho, Anita M.; Cashman, Katharine V. (1997) Temperature constraints on the Ginkgo flow of the Columbia River Basalt Group. *Geology* 25: 403–406.

Hoblitt, Richard P.; Orr, Tim R.; Heliker, Christina; Denlinger, Roger P.; Hon, Ken; Cervelli, Peter F. (2012) Inflation rates, rifts, and bands in a pāhoehoe sheet flow. *Geological Society of America* 8:179-195.

Hon, Ken; Kauahikaua, Jim; Denlinger, Roger; MacKay, Kevin (1994) Emplacement and inflation of pahoehoe sheet flows: Observations and measurements of active lava flows on Kilauea Volcano, Hawaii. *Geological Society of America Bulletin* 106:351-370.

Keszthelyi, Laszlo; Jaeger, Windy; McEwen, Alfred; Tornabene, Livio; Beyer, Ross A.; Dundas, Colin; Milazzo, Moses (2008) High Resolution Imaging Science Experiment (HiRISE) images of volcanic terrains from the first 6 months of the

Mars Reconnaissance Orbiter Primary Science Phase. *Journal of Geophysical Research* 113.

Mabery, M. V., R. B. Moore, and K. A. Hon (1999) The volcanic eruptions of El Malpais: a guide to the volcanic history and formations of El Malpais National Monument. Ancient City Press, Santa Fe, New Mexico, USA.

Marshak, Stephen (2012) Earth Portrait of a Planet. 4th ed. New York: W.W. Norton & Company.

Nichols, R.L., 1939, Surficial banding and shark's-tooth projections in the cracks of basaltic lava. *American Journal of Science* 237:188-194.

Nichols, Robert L., 1946, McCartys Basalt Flow, Valencia County, New Mexico. *Bulletin of the Geological Society of America* 57:1049-1086.

Peters, Timothy J.; Menzies, Martin; Thirlwall, Matthew; Kyle, Philip R. (2008) Zuni-Bandera volcanism, Rio Grande, USA—Melt formation in garnet- and spinel-facies mantle straddling the asthenosphere—lithosphere boundary. *Lithos* 102: 295-315.

Renault, J. (1970) Major-element variations in the Potrillo, Carrizozo, and McCarty's basalt fields, New Mexico. *New Mexico Bureau Mines Mineral Resources, Circular* 113, p. 22.

Self, S., Keszthelyi, L., and Thordarson, Th. (1998) The Importance of Pahoehoe. *Annual Review Earth Planet Science* 26: 81-110.

Tanaka, Kenneth L., Skinner Jr., James A., Hare, Trent M. (2005) Geologic Map of the Northern Plains of Mars. *U.S. Geological Survey*.

Thordarson, T. and Self, S. (1998) The Roza Member, Columbia River Basalt Group: A gigantic pahoehoe lava flow field formed by endogenous processes? *Journal of Geophysical Research* 103:27411-27445.

Walker, George PL (1991) Structure, and origin by injection of lava under surface crust, of tumuli, “lava rises”, lava-rise pits”, and lava-inflation clefts” in Hawaii. *Bull Volcanol* 53:546-558.

Wentworth, C.K., and Macdonald, G.A. (1953) Structures and forms of basaltic rocks in Hawaii. *U.S. Geological Survey Bulletin* 994:98.

Werner, Stephanie C. (2009) The global Martian volcanic evolutionary history. *Icarus* 201:44-68.

Wilson, Lionel; Head III, James W. (1994) Mars: Review and Analysis of Volcanic Eruption Theory and Relationships to Observed Landforms. *Reviews of Geophysics* 32:3.